Dalton Transactions

PERSPECTIVE

View Article Online
View Journal | View Issue

Cite this: *Dalton Trans.*, 2018, **47**, 8841

Heterometallic 3d–4f single molecule magnets containing diamagnetic metal ions

Amit Chakraborty,[a,b,c] Joydeb Goura,[a,b] Pankaj Kalita,[a] Abinash Swain,[d] Gopalan Rajaraman [d] and Vadapalli Chandrasekhar *[b,c]

Molecular nano magnets such as single-molecule magnets (SMMs) are a class of coordination complexes with numerous potential applications such as information storage devices, Q-bits in quantum computing and spintronics materials. One of the greatest challenges in taking these molecules to end-user applications lies in devising strategies to control and predict their magnetic properties. In this regard, lanthanide-based compounds are very attractive as they possess appealing magnetic properties such as very high barriers for magnetization reversal, very large blocking temperatures *etc*. Controlling the microscopic energy levels of lanthanide-based single-ion magnets (SIMs) is a challenging task and to obtain molecules having very large blocking temperatures, it is desirable to enhance the ground state-excited state gap between the m_J levels and also to quench the quantum tunnelling of magnetization that often circumvents the barrier height. One of the strategies that has been developed by us and others in this area is to employ a diamagnetic transition metal ion to achieve this goal. Over the years several diamagnetic ions such as Zn^{II}, Ni^{II} (square planar), Al^{III} and Co^{III} have been successfully employed to obtain lanthanide-based SMMs with interesting properties. In this perspective, we discuss how incorporation of diamagnetic ion(s) in the cluster aggregation enhances the barrier height for magnetization reversal and hence improves the magnetic properties. We also discuss theoretical studies on such systems based on *ab initio* calculations performed using CASSCF level of theory. Such studies are helpful in affording an understanding of the role and limitation of the diamagnetic ions in enhancing the barrier height for magnetization reversal of molecular nanomagnets.

Received 10th May 2018,
Accepted 14th June 2018

DOI: 10.1039/c8dt01883a

rsc.li/dalton

I. Introduction

Molecular magnets are defined as having a non-vanishing magnetic dipole moment, whether it is permanent or produced by an external field.[1] Because of historic reasons involving the discovery of single-molecule magnet behavior in $[Mn_{12}O_{12}(OAc)_{16}(H_2O)_4]\cdot 2HOAc\cdot 4H_2O$,[1e] molecular magnets have been generally considered as exchange-coupled clusters containing paramagnetic metal centers which are encapsulated by a sheath of organic ligands. The organic sheath prevents intermolecular magnetic interactions between the metal complexes. The exchange interaction between such metal ions is mediated by the bridging coordinating atoms of appropriate ligands.[2]

Molecular magnets have attracted considerable interest among physicists, chemists and material scientists due to their wide range of potential applications which include: ultra-high-density magnetic data storage devices,[3] magnetic refrigeration (high magnetocaloric effect),[4] spintronics[5] and quantum computation.[6] These molecules are also important for understanding several quantum phenomena such as quantum tunneling of the magnetization,[7] spin parity,[8] quantum phase interference, *etc*.[9]

Although the original discovery of SMM behavior was in polynuclear transition metal clusters,[1e] very soon this phenomenon was found in certain heterometallic 3d/4f[10] and homometallic 4f complexes.[11] Among the latter family are complexes, $[Dy(Cp^{ttt})_2][B(C_6F_5)_4]$,[12a,b] and $[L_2Ln(H_2O)_5][I]_3\cdot L_2\cdot(H_2O)$ [Ln = Dy, Er; L = (^{t}BuPO(NH^{i}Pr)$_2$)][13] of which the former (shown in Fig. 1) shows the highest blocking temperature (60 K) to date.

Among various 3d/4f complexes studied, paramagnetic transition metal ions have generally been employed because of the considerations of increasing the ground state spin of the mole-

[a]*School of Chemical Sciences, National Institute of Science Education and Research Bhubaneswar, Jatni, Khurda – 752050, Odisha, India*
[b]*Department of Chemistry, Indian Institute of Technology Kanpur, Kanpur-208016, India. E-mail: vc@niser.ac.in, vc@iitk.ac.in, vc@tifrh.res.in*
[c]*Tata Institute of Fundamental Research Hyderabad, Gopanpally, Hyderabad-500 107, India*
[d]*Department of Chemistry, Indian Institute of Technology Bombay, Powai, Mumbai-400 076, India*

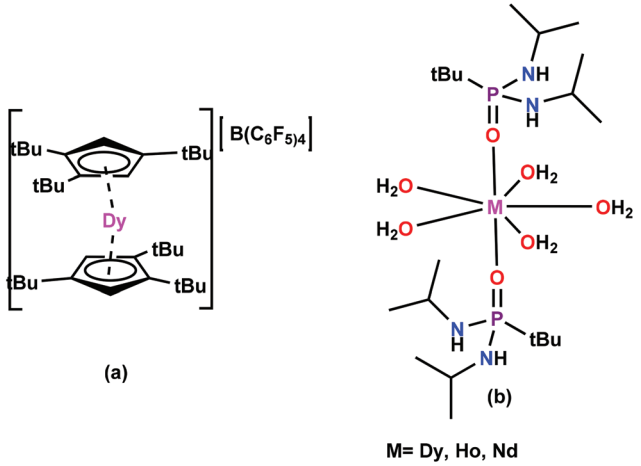

Fig. 1 Chemical structure of mononuclear lanthanide complexes.[12,13] Complex in the left[12a] (a) shows the highest blocking temperature to date.

cule (see below). This perspective deals with 3d/4f complexes where the 3d metal ion is, counter intuitively, diamagnetic. A related class of compounds dealing with 3p/4f metal complexes has also been described.[14] Before dealing with the subject matter of this article a brief background is presented.

Among complexes that contain 3d[15] or 3d/4f[10] metal ions, the prerequisites for a molecular magnet include possessing (a) a high-spin ground state (S) and (b) a high zero-field splitting (ZFS) (due to high magnetic anisotropy, D). Spin–orbit coupling, structural distortions and spin–spin interactions are the three major factors that control the ZFS in a molecular system.[16] The combined effect of S and D, produces an energy barrier (U_{eff}) which is termed as the effective energy barrier for the reversal of magnetization and can be obtained from the equations: $U_{eff} = S^2|D|$ and $U_{eff} = (S^2 - 1/4)|D|$ which are valid for integer and half integer spins, respectively. The SMM behavior of the molecule can be indicated by temperature-dependent out-of-phase AC susceptibility signals as well as by characteristic hysteresis loops in the M *vs.* H plots. Hysteresis for molecular magnets signifies that the magnetization of each molecule is relaxing slowly compared to the sweep rate of the field.[17] Thus, the magnetization of the molecular magnet in the sample never attains the equilibrium value in the time-window of the experiment, resulting in the magnetization getting blocked below certain temperature, called the blocking temperature, T_B. Below the blocking temperature, an SMM possess hysteresis loops in the magnetization (M) *vs.* field (H) plots, revealing a permanent magnetic property and this strongly depends upon the sweep-rate of the magnetic field.[17]

Slow relaxation of magnetization is the signature of SMM behavior and may occur *via* a number of processes through the ground state or *via* an excited state.[18] It is observed that, for lanthanide-containing SMMs, a temperature-independent region, usually possessing fast relaxation of the magnetization *via* quantum tunneling (QTM), and coexistence of thermal mechanism with the QTM results in a curvature in the Arrhenius plot of $\ln \tau$ *vs.* $1/T$. Thus, the coexistence of thermal mechanism can be calculated by examination of the so-called Argand or Cole–Cole plots, where χ'' (out of phase susceptibility) is plotted against χ' (in phase susceptibility) at a constant temperature, providing a semi-circular representation for an ideal single-mechanism relaxation. Besides this, magnetic relaxation can also be phonon-assisted in either a two phonon process (Orbach, Raman) or a one-phonon process (direct). Orbach processes proceed through the absorption of a phonon, resulting in an excitation to a real state followed by

Amit Chakraborty

Amit Chakraborty obtained his B.Sc. degree from the Suri Vidyasagar College, Burdwan University, West Bengal, India, in 2007 and M.Sc. degree in 2009 in inorganic chemistry from Indian Institute of Technology Kanpur, Kanpur, India. He has completed his Ph. D. at Indian Institute of Technology Kanpur, Kanpur, India, under the supervision of Prof. V. Chandrasekhar in 2015. He briefly worked as a postdoctoral research associate at the National Institute of Science Education and Research (NISER), Bhubaneswar, India. Currently he is a National Post-doctoral Fellow at the Tata Institute of Fundamental Research Hyderabad. His research interests include molecular magnetism, transition metal/lanthanide complexes, design of unusual ligands and in new molecular materials.

Joydeb Goura

Joydeb Goura, was born in 1986 and received his Ph.D in 2014 from Indian Institute of Technology Kanpur, India, under the supervision of Prof. V. Chandrasekhar. He was a postdoctoral research associate at the National Institute of Science Education and Research (NISER), Bhubaneswar. Afterwards, he briefly worked at the University of Göttingen with Prof. H. W. Roesky, before moving to work with Prof. F. Jaekle at Rutgers University-Newark, USA after obtaining a SERB Indo-US Postdoctoral Fellowship. Since October, 2017, Joydeb is a postdoctoral fellow at the Jacobs University-Bremen in the group of Prof. Ulrich Kortz. His current area of research includes the synthesis and properties of mixed 3d/4f metal-containing polyoxometalates (POMs).

emission of a phonon and relaxation. On the other hand, a Raman process involves the absorption of a phonon providing the excitation of a spin to a virtual level, followed by relaxation and emission of a phonon. A direct process leads to the spin flipping of the molecule with the emission of a phonon.[10]

II. 3d/4f complexes as SMMs

The realization that most trivalent lanthanide ions (except Gd^{III}) possess a large single-ion anisotropy due to their unquenched orbital angular momentum as well as a large ground state spin prompted their incorporation in heterometallic complexes.[10] In homometallic polynuclear Ln^{III} complexes, the magnetic interactions between the "f" electrons of different metal centers are very small. On the other hand, among heterometallic complexes, the magnitude of exchange interactions among the 3d–4f metal ions is usually larger than those present in 4f–4f interactions and the problem of orbital degeneracy may be limited.[10] Accordingly, the first 3d/4f SMM, a $Cu^{II}_2Tb^{III}_2$ complex was reported by Osa and co-workers in 2004 (Fig. 2).[19] This complex was synthesized by using the ligand, 1-(2-hydroxybenzamido)-2-(2-hydroxy-3-methoxy-benzylideneamino)-ethane. Magnetic measurements of this compound reveal a ferromagnetic interaction (θ = 14.3 K) between Cu^{II} and Tb^{III} ions. This compound was shown to be an SMM with an energy barrier, U_{eff} = 21 K with $\tau_0 = 2.7 \times 10^{-8}$ s. However, hysteresis was not observed for this compound even up to 2 K; the estimated blocking temperature T_B being 1.2 K.[19]

Although, the initial research regarding 3d–4f chemistry mainly focused on Cu^{II}/Ln^{III} complexes, [for a representative example, see Fig. 3(a)], very soon combination with other transition metal ions was investigated. In this context, the first Co^{II}–Ln^{III} based SMM, $[LCo^{II}–Gd^{III}–Co^{II}L]^+$, ($LH_3$ = (S)P[N(Me)N=CH–C_6H_3–2-OH–3-OCH_3]$_3$), a cationic trinuclear complex, was reported by some of us in 2007 [Fig. 3(b)].[20] Magnetic

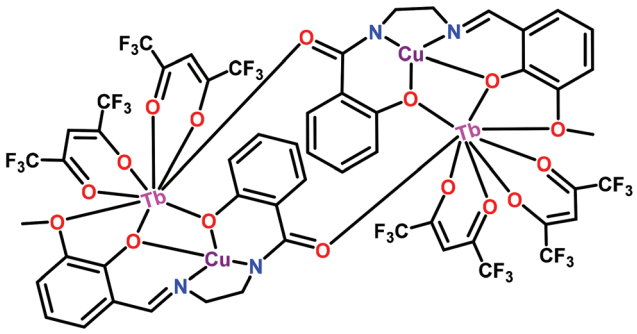

Fig. 2 Chemical structure of first reported 3d/4f complex (Cu^{II}_2/Tb^{III}_2) that was shown to be an SMM.[19]

studies of this compound revealed a ferromagnetic exchange interaction between Co^{II} and Gd^{III}. Magnetization *versus* field studies suggested an effective spin ground state of S = 9/2. This compound showed slow magnetic relaxation below 8 K in AC susceptibility measurements. Analysis of the frequency dependent out-of-phase (χ'') signal reveals an energy barrier (U_{eff}) = 27 K and $\tau_0 = 1.7 \times 10^{-7}$ s. It may be noted that although Gd^{III} is isotropic, the anisotropy of this complex arises due to the orbital contribution from the Co^{II} ions and hence behaves as a SMM. We have reported many other 3d/4f complexes with various 3d and 4f metal ions.[21,22]

Several types of 3d/4f complexes have since been reported, representative examples of which along with their magnetic properties are given in Table 1.

III. Single-molecule magnets containing diamagnetic metal ions

As mentioned above, for a majority of 3d–4f complexes, paramagnetic 3d and 4f metal ions have been used with a

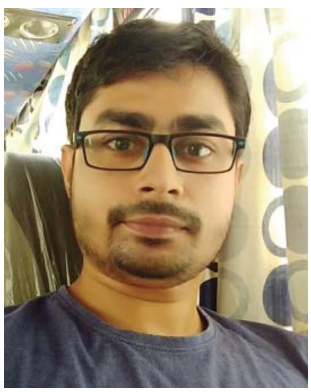

Pankaj Kalita

Pankaj Kalita has obtained his B.Sc. degree from the B. Borooah College, Gauhati University, Guwahati, Assam, India in 2012 and M.Sc. degree in 2014 in inorganic chemistry from Gauhati University, Assam, India. He is currently pursuing his Ph.D. under the supervision of Prof. Vadapalli Chandrasekhar at the National Institute of Science Education and Research (NISER), Bhubaneswar, India. His research focuses on the synthesis, structure and magnetism of mononuclear lanthanide complexes, and heterometallic 3d/4f complexes.

Abinash Swain

Abinash Swain was born in Bargarh (Odisha), India and received a BSc in Chemistry from BJB College, Utkal University, Bhubaneswar in 2013. He obtained his MSc from School of Chemistry, University of Hyderabad in 2015 and received UGC-JRF scholarships to undertake a PhD under the supervision of Prof. Gopalan Rajaraman at IIT Bombay, India. His research interests are in the area of lanthanide based magnets, particularly exploring novel toroidal systems. He pursued both the synthesis of novel lanthanide clusters and modelling the same using ab initio *calculations, in search of ferrotoroidic Ln clusters.*

view to increase the ground state spin S. In a contrary approach heterometallic complexes containing diamagnetic metal ions such as, Zn^{II},[23] Mg^{II},[24] Ca^{II},[25] Al^{III},[14] low-spin Co^{III},[26] square-planar Ni^{II} [27] along with Ln^{III} ions have been investigated. Interestingly, it is seen that these diamagnetic cations influence the electron density distribution of the surrounding coordinating ligands around the lanthanide ion and help in augmenting the SMM properties of such complexes.[28] Theoretical work, particularly on Zn^{II}/Ln^{III} complexes[28,29] has revealed that the diamagnetic metal ion influences and increases the negative charge on the bridging oxide centers (between the diamagnetic metal ion and the 4f metal ion) and stabilizes the ground state of the lanthanide metal ions. As a result, the energy barrier for the reversal of magnetization increases. Given this background, we now proceed to describe some of the systems that have been investigated.

III.1 Ligands used

In order to achieve appropriate nuclearity and topology of 3d/4f complexes containing diamagnetic metal ions we have designed several ligands. Those that are relevant to the theme of this perspective are given in Chart 1. As can be seen, most of these are polytopic ligands and are built from a Schiff- or a Mannich-type condensation. Almost all of the ligands have potential phenolate coordinating sites which in most instances acts as a bridging ligand between the metal centre. Further, many of the ligands such as **1–7** and **12–13** can be considered as compartmental ligands with sites for specific ligation towards a transition or a lanthanide metal ion.

III.2. Synthesis of M^{II}/Ln^{III} [M = Zn, Mg] complexes and their magnetic properties

Before we present our work in this field relevant examples from the literature are described. Essentially many of the com-

Gopalan Rajaraman

Gopalan Rajaraman (born in Thanjavur, India) after completing his Masters from Bharathidasan University, Trichy, India, moved to the University of Manchester, U. K. for his PhD under the supervision of Prof. R. E. P. Winpenny and Dr E. J. L. McInnes. After obtaining his Ph.D in 2004, he undertook postdoctoral stays at the University of Heidelberg, Germany (2005–2007) in the group of Prof. P. Comba and the University of Florence, Italy in the group of Prof. D. Gatteschi (2007–2009). He joined IIT Bombay, India as an assistant professor in December, 2009 and became an associate professor in 2014. His research focuses on employing electronic structure methods to understand the structure, properties and reactivity of molecules possessing unpaired electrons (open-shell systems). In addition to modelling molecular magnets, his group also actively pursues research in the area of modelling bio-mimic reactions catalysed by high-valent metal-oxo/imido complexes.

Vadapalli Chandrasekhar

Vadapalli Chandrasekhar was born in Kolkata in November 1958. After his early education at the Osmania University, Hyderabad, he obtained his Ph.D. degree in 1982 from the Indian Institute of Science, Bangalore. He did his postdoctoral work at the University of Massachusetts, Amherst, MA (1983–1986). After briefly working at the Research and Development section of the Indian Petrochemicals Corporation at Vadodara, as a Senior Research Officer, he joined the Department of Chemistry at the Indian Institute of Technology Kanpur in 1987 where he has been a full professor since 1995. He served as the Head of the Department of Chemistry, IIT Kanpur (2008–10), and as the Dean of Faculty Affairs, IIT Kanpur (2011–12). He was the Director of the National Institute of Science Education and Research (NISER), Bhubaneswar, India (2014–17). Currently he is the Centre Director, Tata Institute of Fundamental Research, Hyderabad. His research interests are in the area of molecular materials, inorganic rings and polymers, main-group organometallics, and polynuclear metal assemblies. He has been a recipient of several national and international awards and fellowships. He received the S. S. Bhatnagar Award of the Council and Scientific Industrial Research, India, and the Friedrich–Wilhelm–Bessel Research Award of the Alexander von Humboldt Foundation, Germany. He is an elected Fellow of the Indian Academy of Sciences, Bangalore, the National Academy of Sciences, Allahabad, the Indian National Science Academy, and the Academy of Sciences of the Developing World, Trieste, Italy. He served on the editorial board of several leading journals including the ACS journal, Organometallics. He is currently on the editorial board of Dalton Transactions.

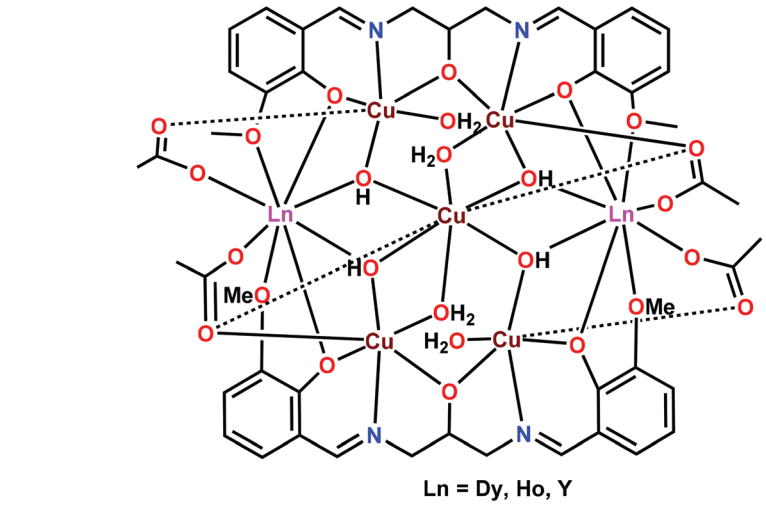

(a)

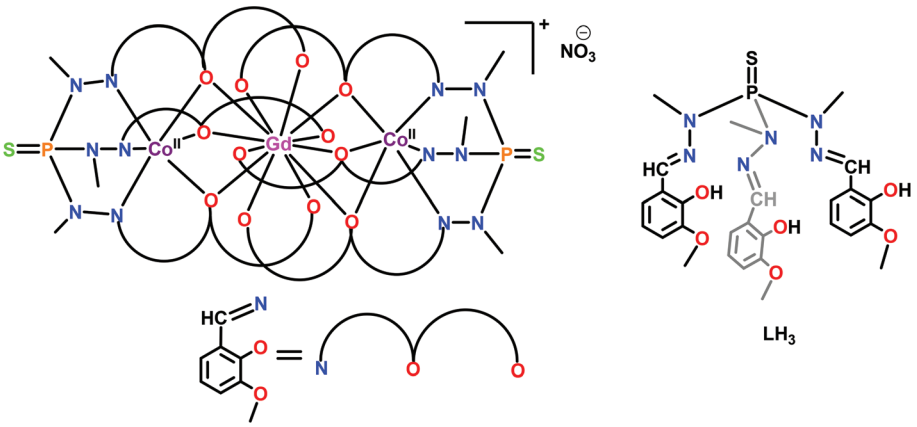

(b)

Fig. 3 Line diagrams of some representative examples of 3d–4f SMMs showing (a) hepta-nuclear $Cu^{II}_5Ln^{III}_2$ complex[21b] and (b) tri-nuclear $Co^{II}_2Ln^{III}$ [20,21d] complexes.

Table 1 Representative examples of 3d/4f SMMs

3d/4f complex	Energy barrier (U_{eff}/K), pre-exponential factor (τ_0/s)	Ref.
$[Cr^{III}_4Dy^{III}_4(\mu_3\text{-}OH)_4(\mu\text{-}N_3)_4(mdea)_4(piv)_4]$ 3 CH_2Cl_2 H_2mdea = methyldiethanolamine	U_{eff} = 15, $\tau_0 = 1.9 \times 10^{-7}$	22*a*
$[Mn^{III}_6Tb^{III}_2O_3(OMe)_6(HOMe)_4$ (sao)$_6(H_2O)_2]$	U_{eff} = 103, $\tau_0 = 1.6 \times 10^{-10}$	22*b*
$[Fe^{III}_6Dy^{III}_3(\mu_7\text{-}C_2H_2O_4)$ $(\mu_4\text{-tea})_2(\mu_3\text{-teaH})_4(\mu_2\text{-}N_3)_2$ $(N_3)_6$ $(NO_3)]$ 2EtOH ($C_2H_2O_4^{4-}$ = tetra anion of 1,1,2,2-tetrahydroxyethane)	U_{eff} = 65.1, $\tau_0 = 1.64 \times 10^{-12}$	22*c*
$[L_2Co^{II}_2Gd^{III}]NO_3$ H_3L = (S)P[N(Me)N = CH–C_6H_3-2-OH-3-OMe]$_3$	U_{eff} = 27.4, $\tau_0 = 1.5 \times 10^{-7}$	20
$[Co^{II}_2Dy^{III}_2(L)_4(NO_3)_2(THF)_2]\cdot 4THF$ H_3L = ((*E*)-2-(2-hydroxy-3-methoxybenzylideneamino)phenol)	U_{eff} = 117.28, $\tau_0 = 6.2 \times 10^{-7}$	22*d*
$Ni^{II}_2Dy^{III}_2L_{10}(bipy)_2$ L = 3,5-dichlorobenzoic acid	$U_{eff}1$ = 105, $\tau_0 = 1.8 \times 10^{-11}$; $U_{eff}2$ = 73, $\tau_0 = 1 \times 10^{-12}$	22*e*
$[\{Cu^{II}(dpk)_2\}\{Tb^{III}(hfac)_3\}_2]$ hfac = hexafluoroacetylacetone	U_{eff} = 47, $\tau_0 = 1.1 \times 10^{-7}$	22*f*

plexes that would be described possess only one paramagnetic ion in the form of the lanthanide ion. Such systems can also be termed as single-ion magnets (SIMs). It is well known that SMM behavior originating from single ion lanthanide complexes is caused due to interaction of ground spin–orbit coupled *J*-state with the crystal field.[30] Thus, fine-tuning the

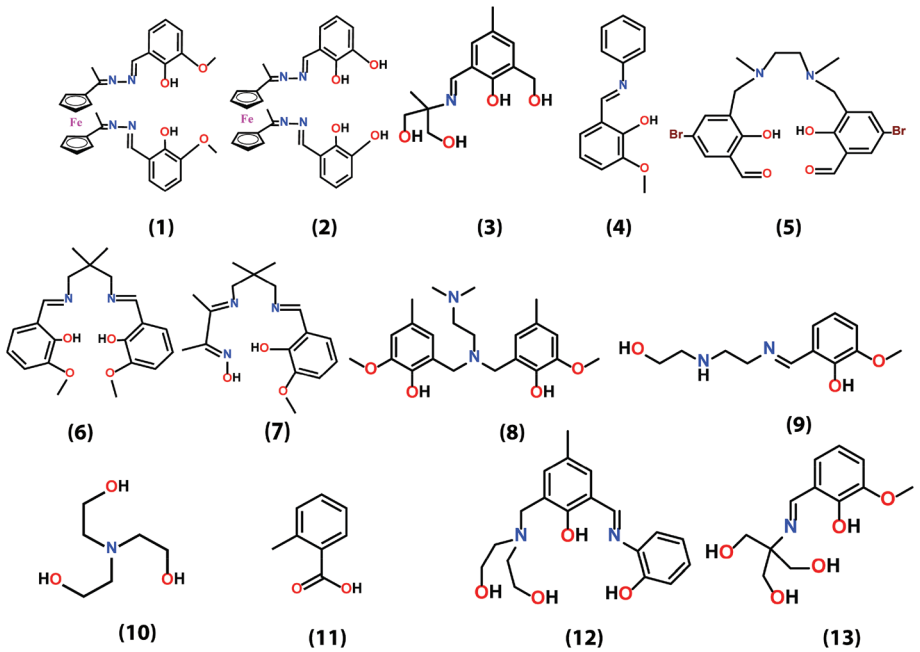

Chart 1 Various polytopic ligands used for preparing 3d/4f complexes that are discussed in this article.

local symmetry and crystal field around lanthanide ions is an effective strategy to promote blocking temperatures of SIMs. It has been observed that, a relatively high local symmetry (D_{4d}, D_{3h}, D_{2d}, D_{5h}, C_5, and C_∞) around the lanthanide ions could suppress the tunneling of the magnetization (QTM) and produce a significant magnetic anisotropy.[29] Besides this, maximizing the single ion magnetic anisotropy (oblate f-electron density for Tb^{III} and Dy^{III} ions) or (prolate type for Er^{III} ions) of the lanthanide ions is an important objective in designing the complexes.[28,29] Thus, combination of diamagnetic 3d metal ion such as Zn^{II} and anisotropic lanthanide ion often leads to greater electrostatic interaction in the g_{zz} axis affording single molecule magnet properties. A number of Zn^{II}/Ln^{III} complexes using various Salen type ligands as well as other multisite coordinating ligands, have been synthesized and their magnetic properties, explored (Table 2). In this regard, use of Mg^{II} as a diamagnetic metal ion for the preparation of heterometallic complexes is relatively rare. Some representative examples of Zn^{II}/Ln^{III} [23] and Mg^{II}/Ln^{III} [24] complexes are given in Schemes 1 and 2, Chart 2 and Table 2.

With this background we describe our efforts in this area. Our initial focus was the design of a ferrocene-based compartmental ligand [H_2L (**1**) (Chart 1)] which was utilized for preparing bimetallic Zn^{II}–Ln^{III} complexes (**1a–1f**) (Scheme 3). In these dinuclear systems (Scheme 3) two different metal ions are bound in two different pockets; the transition metal ion occupies the inner coordination pocket and the outer coordination pocket holds the lanthanide ion. A modification of this ligand [H_4L(2), Chart 1] involving the replacement of the terminal methoxy group by cluster propagating hydroxyl group allowed the assembly of the octanuclear $Zn^{II}_4Ln^{III}_4$ complexes (**2a–2c**) (Scheme 3). Magnetic studies of these complexes revealed that these do not show SMM behavior.[30]

In view of the above, we designed a multi dentate ligand H_4L (**3**) (Chart 1) which was synthesized by the condensation of 2-amino-2-methylpropane-1,3-diol with 2-hydroxy-3-(hydroxymethyl)-5-methylbenzaldehyde. Utilizing **3**, it was possible to prepare a series of linear $Mg^{II}_2Ln^{III}$ (Ln^{III} = Dy^{III} (**3a**); Gd^{III} (**3b**); Tb^{III} (**3c**)) and $Zn^{II}_2Ln^{III}$ (Ln^{III} = Dy^{III} (**3d**), Tb^{III} (**3e**) and Gd^{III} (**3f**)) complexes (Scheme 4).

In these complexes, the lanthanide ion occupies the central position and is eight-coordinate in a distorted square antiprism geometry. The magnetic properties of these complexes essentially stem from the single ion properties of the lanthanide ion.[23q]

Complexes $Mg^{II}_2Dy^{III}$ (**3a**) and $Zn^{II}_2Dy^{III}$ (**3d**) show SMM behavior (Fig. 4 and 5 respectively). **3a** reveals a fast and a slow relaxation behavior: U_{eff} = 72(2) K with $\tau_0 = 8 \times 10^{-9}$ s for the slow relaxation process and U_{eff} = 61(2) K with $\tau_0 = 4 \times 10^{-7}$ s for the fast relaxation process. On the other hand complex **3d** reveals a single relaxation process: U_{eff} = 67(3) K with $\tau_0 = 4.5 \times 10^{-8}$ s. For further investigation for the origin of anisotropy, AC susceptibility measurements were carried out for magnetically diluted samples of Mg^{II}/Dy^{III} and Zn^{II}/Dy^{III}, (Dy^{III}/Y^{III} molar ratio of 1 : 10). This revealed that the relaxation dynamics was not due to intermolecular interactions and/or long range ordering and is essentially of single molecular origin. It may be mentioned that the diluted compounds ($Mg^{II}_2Dy^{III}/Mg^{II}_2Y^{III}$) (**3a′**) and ($Zn^{II}_2Dy^{III}/Zn^{II}_2Y^{III}$) (**3d′**) exhibit SMM behavior under zero magnetic field. Presence of quantum tunneling of magnetization (QTM) is also revealed [U_{eff} = 66(7) K with $\tau_0 = 1.7 \times 10^{-8}$ s and τ_{QT} = 0.0017(1) s, and U_{eff} = 72(3) K with $\tau_0 = 1.2 \times 10^{-8}$ s and τ_{QT} = 0.0004(2) s for

Table 2 A summary of representative examples of Zn^{II}/Ln^{III} SMMs

Complex	Energy barrier (U_{eff}/K), pre-exponential factor (τ_0/s)	Ref.
$[Zn^{II}(\mu\text{-L})(\mu\text{-}NO_3)Yb^{III}(NO_3)_2]$	U_{eff}: 27.0 K τ_0(s) = 8.8×10^{-7}	23*a*
$[Zn^{II}(\mu\text{-L})(\mu\text{-9-An})Dy^{III}(NO_3)2]\cdot 2CH_3CN$ An = anthracene carboxylic acid	U_{eff}: 32.1 K τ_0(s) = 1.9×10^{-6}	23*b*
$[Zn^{II}(\mu\text{-L})(\mu\text{-}NO_3)Er^{III}(NO_3)_2]$	U_{eff}: 22 K (1000) τ_0(s) = 2.0×10^{-6}	23*b*
$[Zn^{II}(\mu\text{-L})(\mu\text{-OAc})Dy^{III}(NO_3)_2]$ L = *N*,*N*′,*N*″-trimethyl-*N*,*N*″-bis(2-hydroxy-3-methoxy-5-methylbenzyl) diethylenetriamine	U_{eff}: 41 K (1000) τ_0(s) = 5.6×10^{-7}	23*b*
$[Zn^{II}Dy^{III}(L)_2(CH_3CO_2)(NO_3)_2]$ (L = 2-methoxy-6-[(*E*) phenyliminomethyl] phenol)	U_{eff}: 83 K (3500 Oe) τ_0(s) = 1.36×10^{-8}	23*c*
$[Zn^{II}(\mu\text{-L})(\mu\text{-OAc})Ln^{III}(NO_3)_2]\cdot CH_3CN$ (Ln^{III} = Nd^{III}, Dy^{III}, Er^{III}, Yb^{III}) (L = *N*,*N*-dimethyl-*N*,*N*-bis(2-hydroxy-3-formyl-5-bromobenzyl)ethylenediamine)	U_{eff}1: 14.12 K and U_{eff}2: 17.10 K (1000 Oe) τ_0(s) = 8.57×10^{-7} and 4.71×10^{-7}, For Nd^{III} U_{eff}: 41.55 K (1000 Oe) τ_0(s) = 1.79×10^{-8}, For Dy^{III}; U_{eff}: 21.0 K (1000 Oe) τ_0(s) = 2.28×10^{-7}, For Er^{III}; U_{eff}1: 18.9 K and U_{eff}2: 23.65 K (1000 Oe) τ_0(s) = 4.59×10^{-6} and 3.79×10^{-6}, For Yb^{III}	23*d*
$[Zn^{II}Ln^{III}(NO_3)_2(mpko)_3(mpkoH)]$ (Ln^{III} = Dy^{III}, Ho^{III}) (mpko = methyl 2-pyridyl ketone oxime)	SMM for Dy^{III} U_{eff}: 33.3 K (1000 Oe) τ_0(s) = 2.0×10^{-7}	23*e*
$[Zn^{II}Ln^{III}(HL\dagger)(NO_3)(OAc)(D)](NO_3)$ (Ln = Tb, D = H_2O; Ln = Dy^{III} and Er^{III}, D = CH_3OH)	SMM for Dy^{III} U_{eff}: 28.53 K (1000 Oe) for τ_0(s) = 2.16×10^{-7}	23*f*
$[Zn^{II}_2Ln^{III}(L\dagger)(NO_3)_2(OAc)_2(H_2O)]$ (Ln^{III} = Dy^{III} and Er^{III}) HL† is shown in Chart 3	U_{eff}: 33.14 K (1000 Oe) τ_0(s) = 4.60×10^{-7} for Dy^{III} U_{eff}: 20.81 K (1000 Oe) τ_0(s) = 7.48×10^{-7} for Er^{III}	23*f*
$[Zn^{II}Cl(\mu\text{-L}')Ln^{III}(\mu\text{-L}')ClZn^{II}][Zn^{II}Cl_3(CH_3OH)]\cdot 3CH_3OH$ (Ln^{III} = Dy^{III} and Er^{III}) L′ = *N*,*N*′-dimethyl-*N*,*N*′-bis(2-hydroxy-3-formyl-5-bromo-benzyl)ethylenediamine	SMM behaviour for Dy^{III} analogue Hysteresis at 2 K Butterfly(18 mT s^{-1}) U_{eff}1: 97 K (0) and U_{eff}2: 103 K (1000 Oe) τ_0(s) = 1.4×10^{-7} and 1.07×10^{-7}	23*g*
$[Zn^{II}_2Dy^{III}_2(L^*)_4(EtOH)_6][ClO_4]_2$ (L* = 3-((2-hydroxy-3-methoxybenzylidene)amino)-2-phenol)	U_{eff}: 10.2 K (3000 Oe) τ_0(s) = 7.1×10^{-6}	23*h*
$[\{Zn^{II}(L'')(AcO)\}_2Ln^{III}]BPh_4\cdot CH_3CN$ Ln^{III} = Tb^{III}, Dy^{III}, Ho^{III}, Er^{III}, Tm^{III} and Yb^{III} (L″ = Schiff base of ethylene diamine + two equivalents of *o*-vanillin)	U_{eff}1: 35 K and U_{eff}2: 7.0 K; τ_0(s) = 1.6×10^{-6} and 4.9×10^{-5} for Tb^{III} U_{eff}1: 22.4 K and U_{eff}2: 6.4 K; τ_0(s) = 5.3×10^{-7} and 2×10^{-5} for Dy^{III} U_{eff}1: 42 K and U_{eff}2: 8.6 K; τ_0(s) = 9×10^{-10} and 1.2×10^{-5} for Er^{III} U_{eff}1: 38.2 K and U_{eff}2: 11.0 K; τ_0(s) = 7.0×10^{-8} and 4.7×10^{-5} for Yb^{III}	23*i*
$[\{Zn(L'')(SCN)\}_2Ln(NO_3)]$ Ln^{III} = Tb^{III}, Dy^{III}, La^{III}, $Tb^{III}_{0.14}La^{III}_{0.86}$ (DL1), and ($Dy^{III}_{0.21}La^{III}_{0.79}$(DL2)) (L″ = Schiff base of ethylene diamine + two equivalents of *o*-vanillin)	SMM behaviour for DL1 U_{eff}: 41.2 K (1000 Oe) τ_0(s) = 7.3×10^{-7} SMM behaviour for DL2 U_{eff}: 133 K (0) and 156 K (1000); τ_0(s) = 3.14×10^{-8} and 1.0×10^{-8} DL = magnetically diluted sample	23*j*
$[M^{II}_2Ln^{III}L^{\#}_2]\cdot 2ClO_4\cdot H_2O$ M = Zn^{II}, Ln^{III} = Dy^{III}, Gd^{III} ($L^{\#}$ = tris(((2-hydroxy-3-methoxybenzyl)amino)ethyl) amine)	SMM for Dy^{III} analogue; a butterfly shaped hysteresis at 2 K; U_{eff}: 124.5 K (2000 Oe); τ_0(s) = 8.33×10^{-7}	23*k*
$[Zn^{II}_2Dy^{III}_2(L^{\ddagger})_4(NO_3)_2(CH_3OH)_2]$ ($L^{\ddagger}$ = (*E*)-2-ethoxy-6-(((2-hydroxyphenyl)imino)methyl)phenol)	U_{eff}1: 54.1 K (0) and U_{eff}2: 66.6 K (1000 Oe); τ_0(s) = 4.59×10^{-6} and 3.79×10^{-6}	23*l*
$[Zn^{II}_2(L''')_2(PhCOO)_2Dy^{III}_2(hfac)_4]$ (L‴ = *N*,*N*′-dimethyl-*N*,*N*′-bis(2-hydroxy-3,5-dimethylbenzyl)ethylenediamine)	U_{eff}: 47.9 K (0); τ_0(s) = 2.75×10^{-7}	23*m*
$[Zn^{II}_3Dy^{III}(L^{\dagger\dagger})(NO_3)_3(MeOH)_3]\cdot 4H_2O$ ($L^{\dagger\dagger}$ = shown in Scheme 1)	U_{eff}: 25.8 K; τ_0(s) = 1.2×10^{-6}	23*n*

diluted sample of **3a**′ and **3d**′ respectively]. After applying a small static field of 1000 Oe on (**3a**′) and (**3d**′), the QTM is almost suppressed due to a combination of field and dilution effects and, as expected, the thermal energy barrier undergoes a slight increase with the concomitant decrease of τ_0 [U_{eff} = 90(7) K and τ_0 = 1.1×10^{-9} for (**3a**′) and U_{eff} = 106(4) K and τ_0 = 5.2×10^{-10} for (**3d**′)]. *Ab initio* calculations, carried out on these complexes confirm that the magnetic anisotropy is uniaxial along the M^{II}–Dy^{III}–M^{II} unit and that the relaxation takes place through the first excited state mainly *via* a thermal-assisted QTM process.

Thus, the introduction of diamagnetic metal ions such as Zn^{II} in a Dy^{III} complex appears to be a good strategy to enhance U_{eff}. This could be due to two factors: (i) the quench-

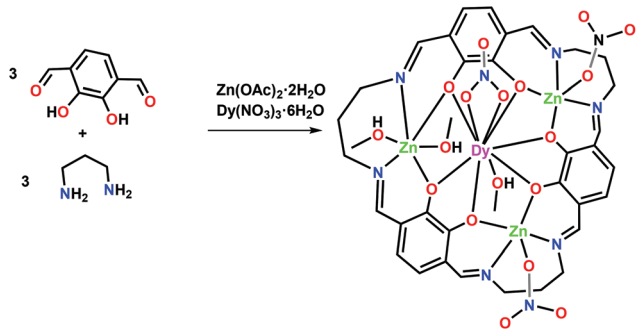

Scheme 1 Synthesis of a tetranuclear $\{Zn^{II}_3Dy^{III}\}$ SMM prepared from a Schiff-base ligand (U_{eff} = 25.8 K).[23n]

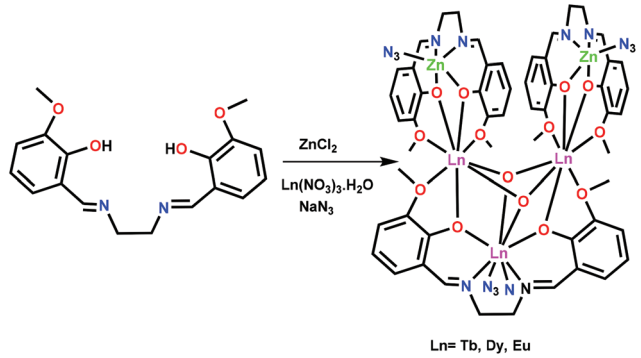

Scheme 2 Synthesis of pentanuclear $\{Zn^{II}_2Ln^{III}_3\}$ SMMs from a Schiff-base ligand (U_{eff} = 13.4 K for Dy^{III} analogue).[23p]

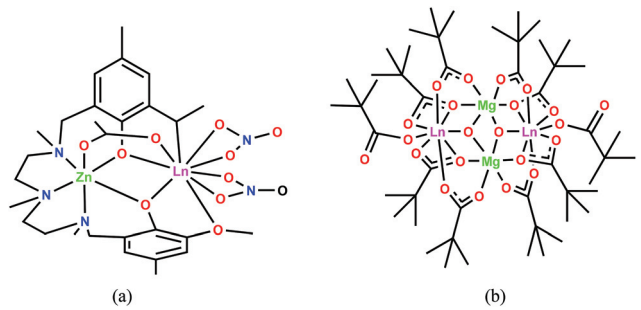

Chart 2 (a) Chemical structure of a dinuclear Zn^{II}/Ln^{III} [23o] based SMM (U_{eff} = 27.5 K and 13.2 K for Dy^{III} and Yb^{III} respectively); and (b) a $Mg^{II}_2Ln^{III}_2$ SMM[24] (U_{eff} = 44 K for Ln = Dy^{III}).

ing of the Ln···Ln interactions promoted by the presence of diamagnetic Zn^{II} ions (internal magnetic dilution) and (ii) the increase of electron density on the donor atoms connecting the Zn^{II} and Dy^{III} ions provoked by the coordination to the Zn^{II} ions.[23c,29c]

Another set of examples where diamagnetic metal ion enables an increasing of the electron withdrawing character of the bridging oxygen atom is provided by a direct comparison of a homometallic $[Dy^{III}\{HL\}_2(NO_3)_3]$ (**4a** and **4b**) and a heterometallic family of complexes $[ZnDy(NO_3)_2\{L\}_2(CH_3CO_2)]$ (**4c**) (Fig. 6) [HL = 2-methoxy-6-[(*E*)-phenyliminomethyl]phenol, Chart 1, compound **4**].[23c,29c]

Complex **4c** consists of Zn^{II} coordinated to the deprotonated L^- ligand (Fig. 6). The effective energy barrier for **4a** and **4c** are estimated to be 16 and 83 K and respectively, the latter being a five-fold increase in the U_{eff} values. *Ab initio* calculations suggests that the *g*-tensors of the ground state doublets are not pure Ising type for **4c** [g_{xx} = 0.02, g_{yy} = 0.04 and g_{zz} = 18.82], while the *g*-tensors for **4a** and **4b** are computed to be of the Ising type (g_{xx} = 0.020, g_{yy} = 0.036, g_{zz} = 19.443 and g_{xx} = 0.081, g_{yy} = 0.121, g_{zz} = 19.092 for **4a** and **4b** respectively) (Fig. 6). Although the *g* tensors tend to worsen upon incorporation of the Zn^{II}, the energy barrier computed clearly reveals the advantage of including Zn^{II} in the cluster.[23c]

To fully comprehend the role of Zn^{II}, DFT calculations were performed and this reveals that the bridging phenoxo oxygen atom in **4c** possess a higher negative charge compared to **4a** (−0.73 *vs.* −0.30). The presence of Zn^{II} cation leads to a larger charge polarization on the oxygen atom, inducing a large electrostatic interaction with the lanthanide ion along the axial direction. This leads to a larger ground-state-excited state gap and hence, enhanced SIM characteristics.[12,13] To arrive at a general conclusion, calculations were performed on several Dy^{III} and Zn^{II}–Dy^{III} SIMs where the enhancement of the ground-state-excited state gap for the Zn^{II} substituted compound is unequivocally established.

Next in this context, is the effect of two Zn^{II} substitutions along with a ligand modification to observe the changes in SMM behavior. One of the important examples in this study is the trinuclear complex $[Zn^{II}Cl(\mu\text{-}L)Ln^{III}(\mu\text{-}L)ClZn^{II}][Zn^{II}Cl_3(CH_3OH)]\cdot 3CH_3OH$ (Ln^{III} = Dy (**5a**) and Er (**5b**)) {H_2L = *N*,*N*′-dimethyl-*N*,*N*′-bis(2-hydroxy-3-formyl-5-bromobenzyl)ethylenediamine (Chart 1, Compound **5**)} (Fig. 7); while **5a** shows an effective energy barrier of 129 K, **5b** does not show any SIM behavior due to its prolate nature.[23g,29a]

Replacing the counter ion has also been found to have an influence in the effective energy barrier. Thus, $[Zn^{II}Cl(\mu\text{-}L)Dy^{III}(\mu\text{-}L)ClZn^{II}]PF_6$ (**5c**) possesses an U_{eff} of 186 K. *Ab initio* calculations reveal that the relaxation occurs *via* second excited state as the molecule preserves a C_2 symmetry.[33] The notable point here is that when the complex containing paramagnetic Ln^{III} is diluted with diamagnetic ion in an isostructural manner, the Ln^{III}–Ln^{III} interaction often decreases and the energy barrier increases.

The *ab initio* calculations yield an energy barrier for **5c** that is almost twice that estimated for **5a**. The energy spectrum shows the energy gap of 144 K from ground to first excited state with pure m_J = 15/2 state and the g_z and $g_{x,y}$ approaching 20 and zero, respectively (Fig. 8).

For **5c**, the estimated U_{eff} is 186 K and this is around 40 K larger than the ground-to-first excited state gap and suggests that the relaxation is possibly happening *via* the second excited state which lies at 243 K. While this would be an overestimated value for magnetization reversal barrier, pronounced QTM effects suggest reduction in the actual barrier as obtained from experiments.[23a,g,31a,33]

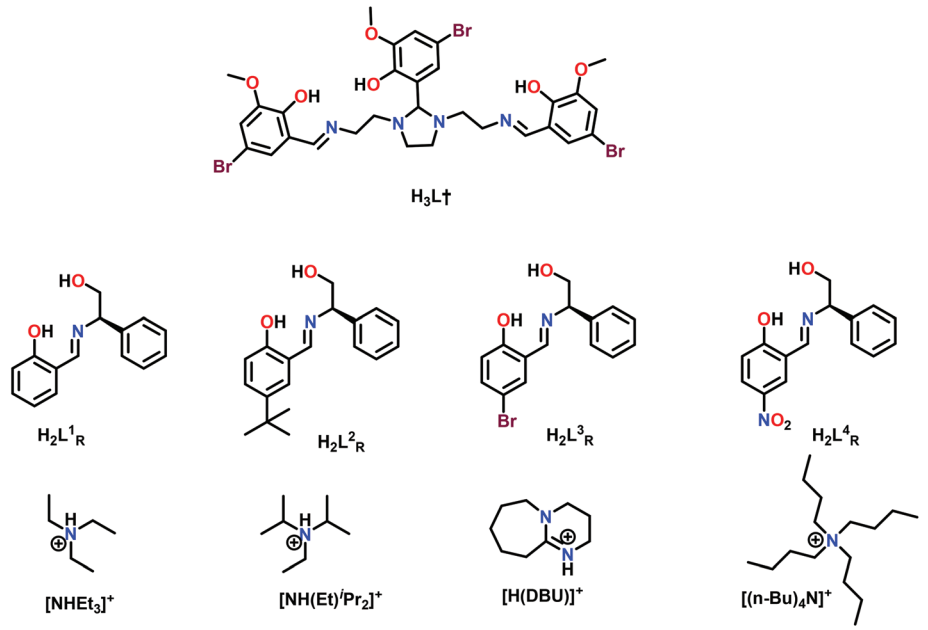

Chart 3 Ligands used for synthesis of Zn^{II}/Ln^{III} (H_3L†)[23f] and Co^{III}–Co^{II} based SMMs.[39a,b]

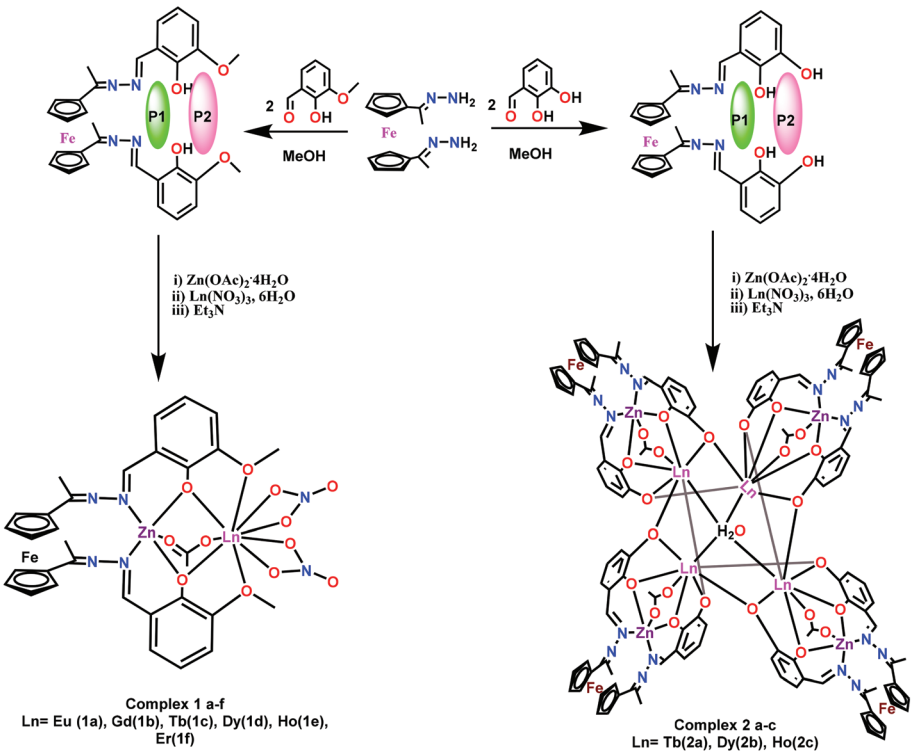

Scheme 3 Synthesis of dinuclear (Zn^{II}/Ln^{III})[30a] and octanuclear (Zn^{III}_4/Ln^{III}_4)[30b] complexes utilizing ferrocene-based compartmental ligands.

A few more complexes of the above kind were reported with different counter anions but having the same trinuclear Zn^{II}–Dy^{III}–Zn^{III} and dinuclear Zn^{II}–Dy^{III} core (Fig. 9 and 10) to observe the effect of counter anion which also appears to be pronounced (Fig. 11).

Utilizing H_2L (**8**) which possesses six potential coordinating donor sites we have isolated a series of $Zn^{II}_3Ln^{III}_3$ (Ln^{III} = Tb^{III} (**8a**) and Dy^{III} (**8b**)) complexes (Scheme 5, Fig. 12). These complexes represent the first examples where the molecular structures reveal a double triangular topology for the $Zn^{II}_3Ln^{III}_3$ core

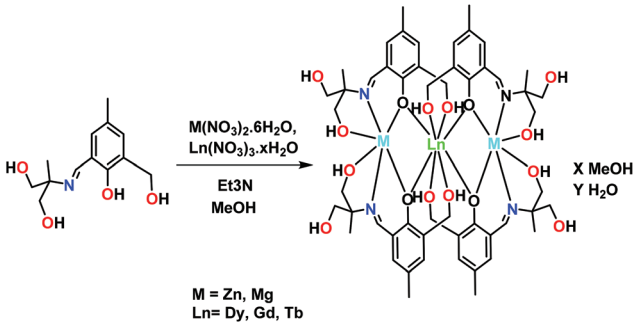

Scheme 4 Synthetic scheme for the preparation of heterometallic $M^{II}_2Ln^{III}$ (M^{II} = Mg^{II} (**3a–3c**) and Zn^{II}) complexes (**3d–3f**).[23q]

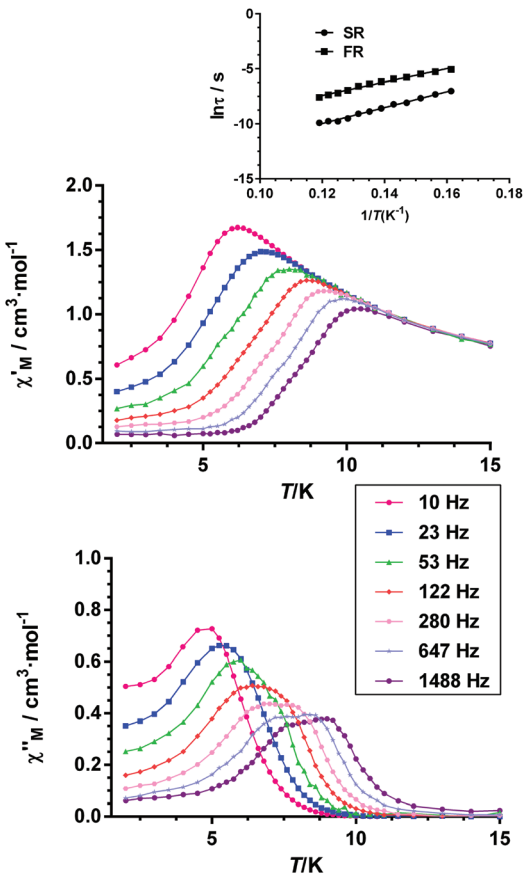

Fig. 4 Temperature dependence of in-phase χ'_M (top) and out-of-phase χ''_M (bottom) components of the AC susceptibility for complex **3a** measured under 1000 Oe applied DC field and Arrhenius plot (inset). Reprinted with the permission from ref. 23*q*. Copyright 2015 Wiley-VCH.

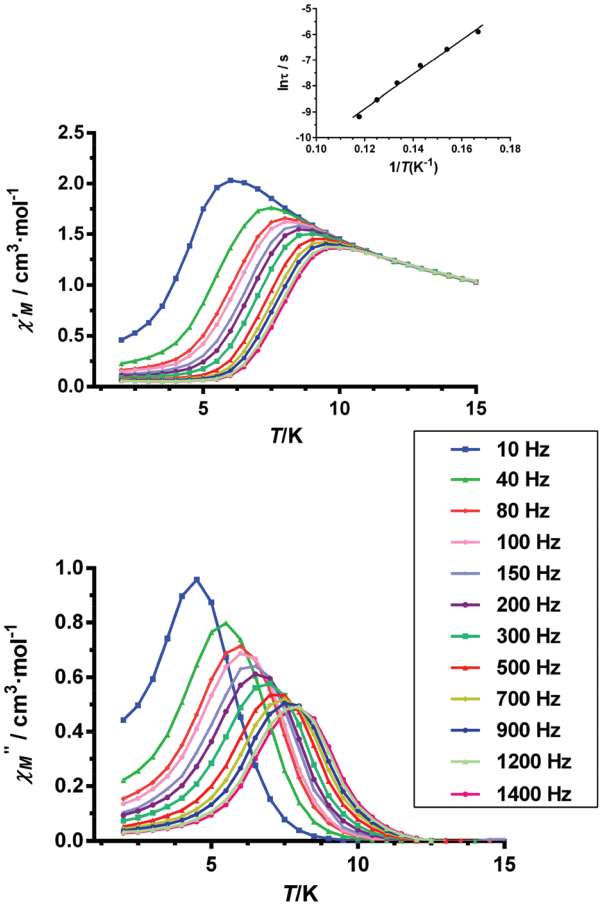

Fig. 5 Temperature dependence of in-phase χ'_M (top) and out-of-phase χ''_M (bottom) components of the AC susceptibility for complex **3d** measured under 1000 Oe applied DC field and Arrhenius plot (inset). Reprinted with the permission from ref. 23*q*. Copyright 2015 Wiley-VCH.

(Fig. 12). An interesting feature of these complexes is that an *in situ* generated carbonate $[CO_3]^{2-}$, holds the three lanthanide centers in a μ-6 fashion. The Zn^{II} center is penta-coordinate in a distorted trigonal bipyramidal geometry while Dy^{III} centers are nine-coordinate in a distorted mono-capped square antiprismatic geometry.[23r]

Theoretical calculations indicate that due to the geometric arrangement of a Dy^{III}_3 triangle, the axial magnetic moments are almost co-planar and tangential to the lanthanide ions defining the equatorial triangle with an almost zero total magnetic moment. This can considered as single-molecule toroics (SMT). Micro-squid measurements on the Dy^{III} counterpart show hysteresis loops below 3 K, which have a S-shape with large coercive fields opening upon cooling, suggesting a SMT behavior.

Magnetic measurements further revealed that due to the ligand field effects, weak intra/intermolecular interactions exist between the lanthanide ions. AC susceptibility measurement on **8b** showed a clear frequency-dependence in the out-of-phase (χ''_M) signals below ~15 K under zero DC field, indicating the existence of slow relaxation of magnetization typical of a single-molecule magnet. At high frequencies (>600 Hz) a maximum at low temperatures (below ~3.5 K) with a shoulder at higher temperatures (above ~6 K) could be observed, which supports the presence of two competing relaxation pathways *via* excited states of the Dy^{III} ions (Fig. 13). The high temperature linear region of the data (between 6.5 K and 10.5 K) could

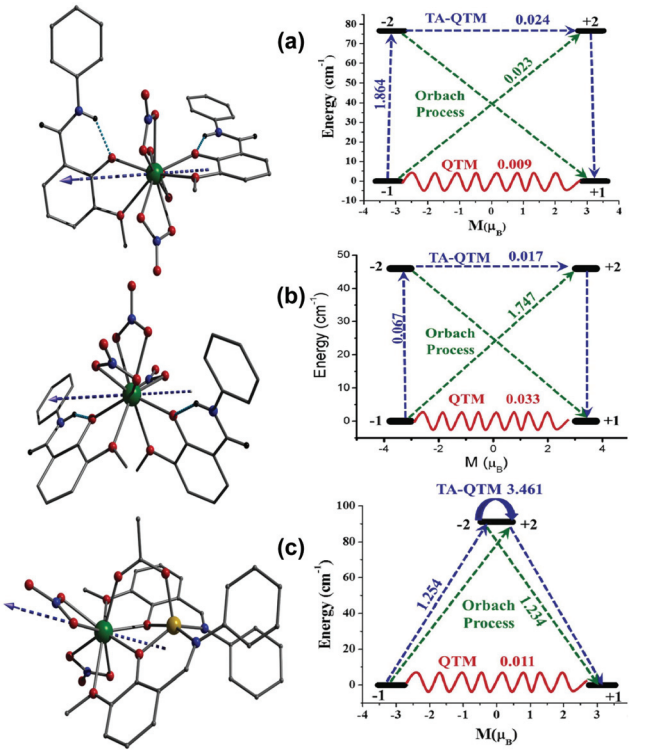

Fig. 6 X-ray structure (left) and *ab initio* calculations-developed mechanism of magnetic relaxation of complexes (a) **4a**, (b) **4b** and (c) **4a**. The blue arrow represents the computed easy axis anisotropy. The sky blue dotted bonds in (a) and (b) represent the intramolecular hydrogen bonding between imine proton and phenolic oxygen of the ligand. Colour code: magenta = Dy^{III}, green = Zn^{II}; red = O; blue = N; grey = C; black = H. Reprinted with the permission from ref. 23c. Copyright 2017 Wiley-VCH.

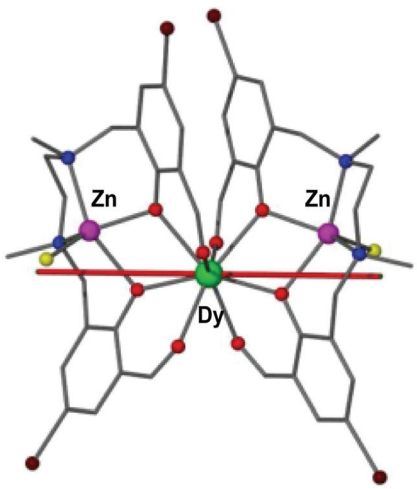

Fig. 7 The trinuclear complex, **5a**, with the representation of the anisotropy axis for the Dy^{III} ion (red line). The local magnetic moment forms an angle with the shorter Dy^{III}–O distances plane of 14.43° and 13.99°, which are close to the direction of that extracted using CASSCF *ab initio* calculations. Adapted from ref. 23g. Reproduced by permission of The Royal Society of Chemistry.

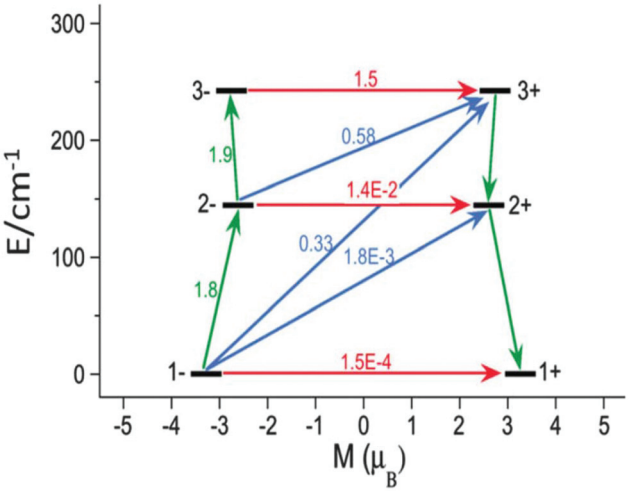

Fig. 8 Energy spectrum of complex **5c**. Three Kramers doublet (KD) as the functions of magnetic moment with *ab initio* computed relaxation pathways. Red = QTM process, blue = Orbach/Raman process, green = TA-QTM. Adapted from ref. 33 with permission of The Royal Society of Chemistry.

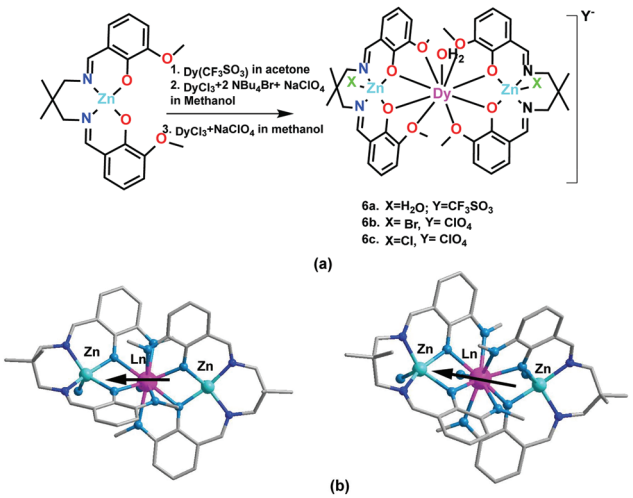

Fig. 9 (a) Preparation of complexes **6a**, **6b** and **6c** utilizing ligand H_2L (**6**). (b) X-ray crystal structures of the corresponding complexes along with the anisotropic direction of the Dy^{III} ion (**6b**, **6c**). (c) Geometry of around the $Dy^{III}O_8$ ion.[23g] Reprinted with the permission from ref. 23g, Copyright 2014 Wiley-VCH.

be fitted to the Arrhenius equation affording an effective thermal energy barrier of 48(1) K and $\tau_0 = 1.0(1) \times 10^{-6}$ s.

III.3. Heterometallic trinuclear bent-geometry containing $Co_2^{III}Ln^{III}$ complexes and $\{Co_2^{III}Ln_2^{III}\}$ butterfly complexes

Heterometallic trinuclear $Co_2^{III}Ln^{III}$ complexes[26a] have been assembled by utilizing a polyfunctional compartmental ligand, 2-methoxy-6-[{2-(2-hydroxyethylamino)ethylimino}methyl] phenol {H_3L(**9**), Chart 1} (Scheme 6, Fig. 14). The metallic core of these complexes consists of a (Co^{III}–Ln^{III}–Co^{III}) motif bridged in a bent geometry resulting in six-coordinated dis-

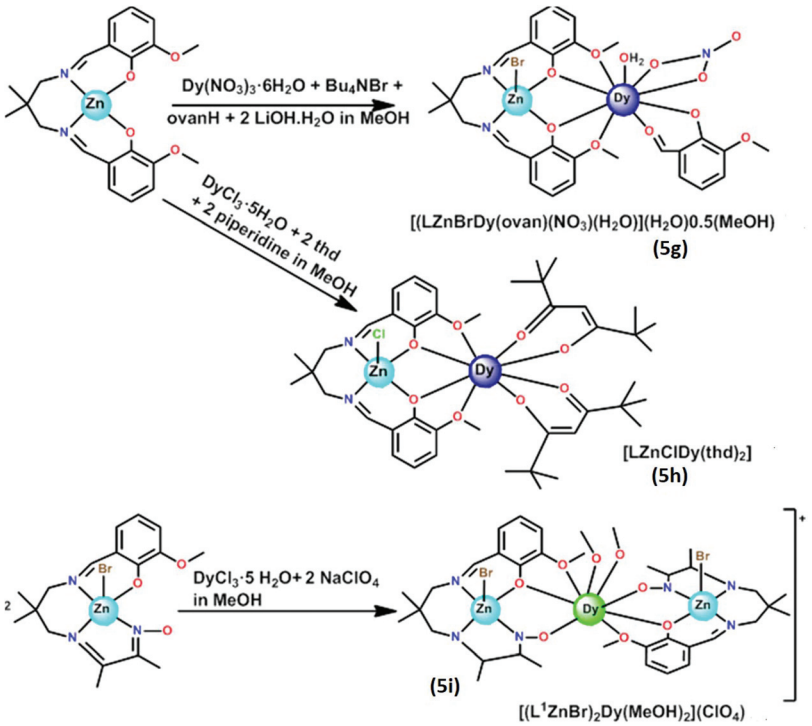

Fig. 10 Dinuclear Zn^{II}–Dy^{III} and trinuclear Zn^{II}–Dy^{III}–Zn^{II} complexes $[(L)Zn^{II}BrDy^{III}(o\text{-van})\ (NO_3)(H_2O)](H_2O)\cdot 0.5(MeOH)(thd)$ (**6d**, **6e**) and $[(LZn^{II}Br)_2Dy\text{-}\ (MeOH)_2](ClO_4)$ (**7a**). The ligands involved are **6** and **7** respectively (see Chart 1). Reprinted with the permission from ref. 32. Copyright 2015 American Chemical Society.

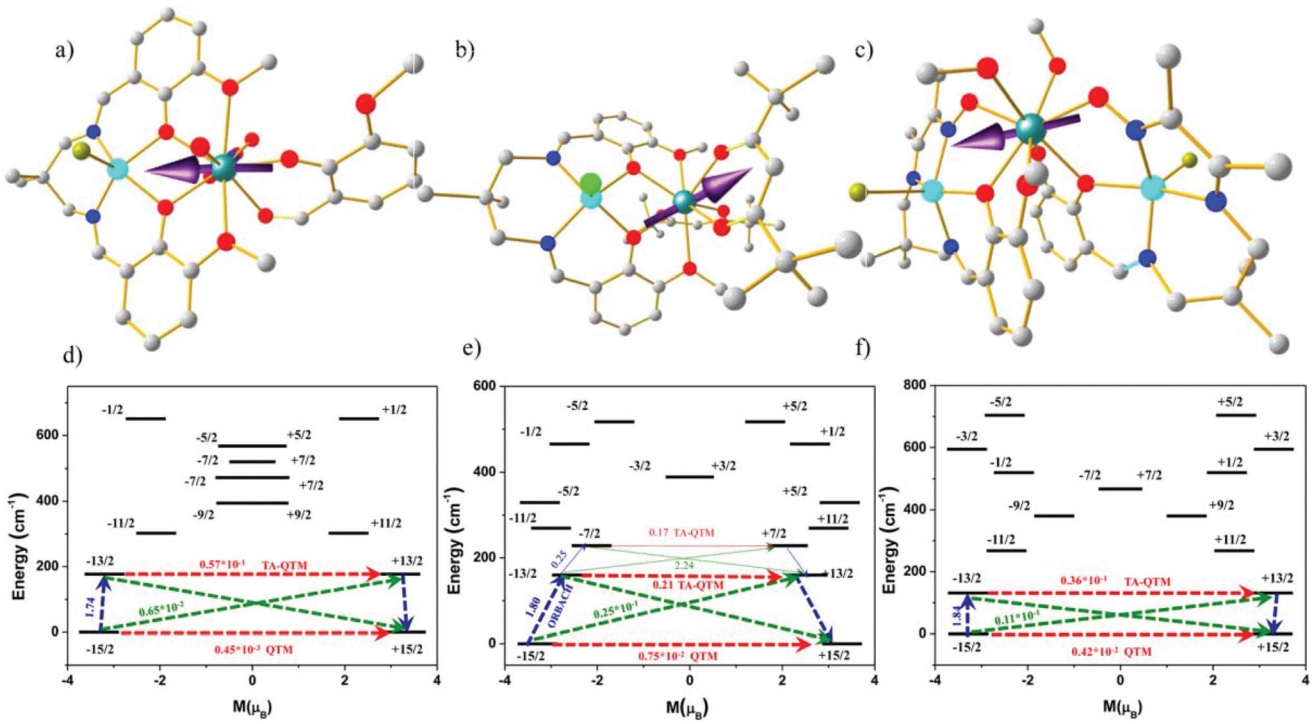

Fig. 11 X-ray structures along with the *ab initio* computed g_{zz} axis for complexes (a) **6a**, (b) **6b**, (c) **7a**. Mechanism of magnetic relaxation developed by *ab initio* calculations for (d) **6a** (e) **6b** and (f) **7a** complexes. Reprinted with the permission from ref. 32. Copyright 2015 American Chemical Society.

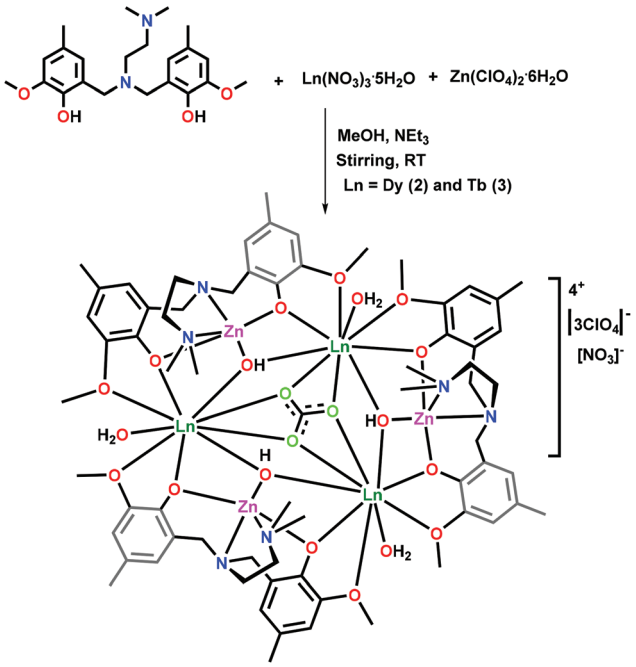

Scheme 5 Synthetic scheme for the preparation of $Zn^{II}_3Ln^{III}_3$ complexes.[23r]

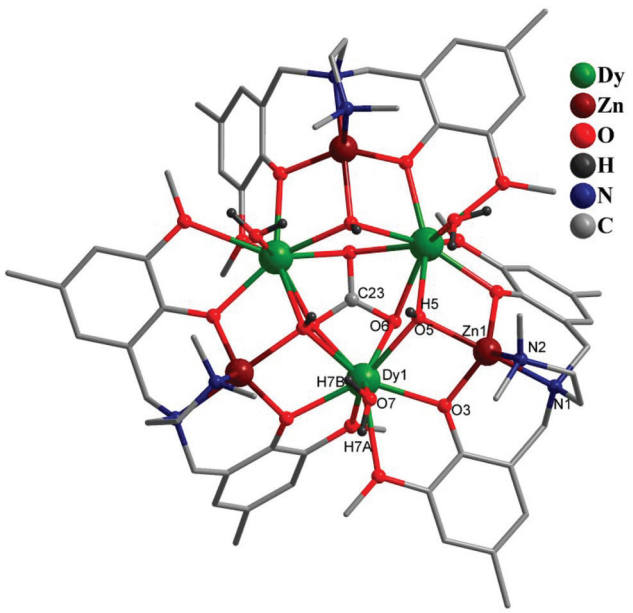

Fig. 12 Solid state molecular structure of the $Zn^{II}_3Dy^{III}_3$ complex, **8b**.[23r] Reprinted with the permission from ref. 23*r*. Copyright 2017 Wiley-VCH.

torted Co^{III} octahedron and a nine-coordinated Ln^{III} monocapped square-antiprisms (Fig. 14). Analysis of the magnetic properties indicates that the Co^{III}_2Dy complex (**9a**) shows a single-ion magnet behaviour. **9a** reveals a large out-of-phase signal in the AC susceptibility measurement at zero DC field below 15 K (Fig. 15) with an energy barrier of 88 K (Table 3 and Fig. 15). The corresponding Er^{III} (**9b**) and Tb^{III} (**9c**) ana-

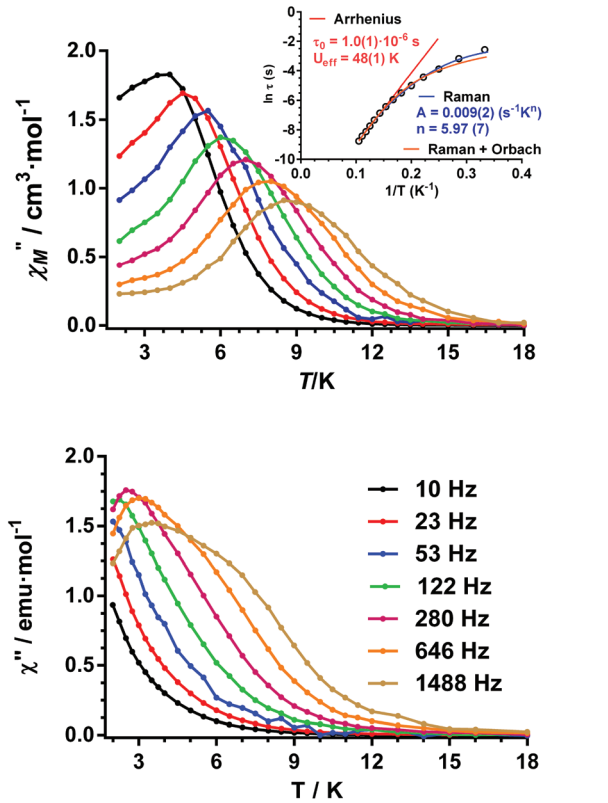

Fig. 13 Temperature dependence of the out-of-phase χ_M'' AC signals under zero DC field (bottom) and 1 kOe (top) for **8b**. Solid lines are guides for the eye. Inset: Arrhenius plots of relaxation times for **8b** under 1 kOe. The red solid line represents the best fitting of the experimental data to the Arrhenius equation, whereas blue and orange lines correspond to the best fitting to the Raman and Orbach plus Raman relaxation processes, respectively. Reprinted with the permission from ref. 23*r*. Copyright 2017 Wiley-VCH.

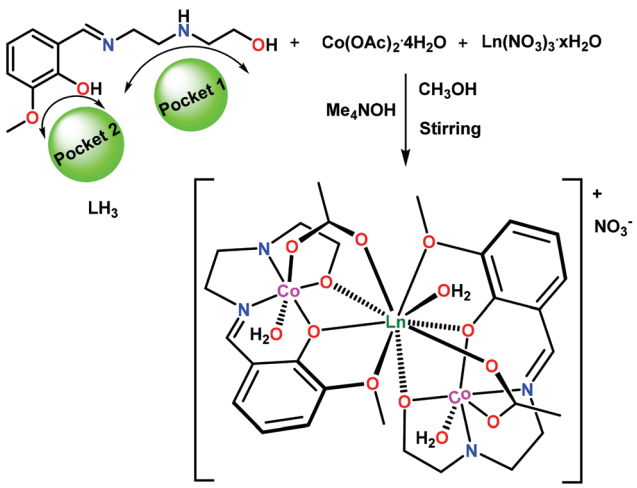

Scheme 6 Synthesis of trinuclear heterometallic $Co^{III}_2Ln^{III}$ complexes.[26a,g]

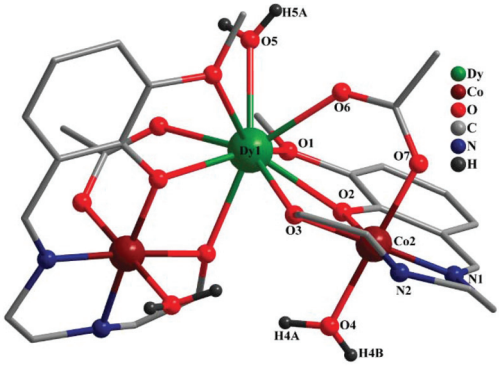

Fig. 14 Molecular structure of $Co^{III}_2Dy^{III}$ (**9a**).[26a] Reprinted with the permission from ref. 26*a*. Copyright 2015 Wiley-VCH.

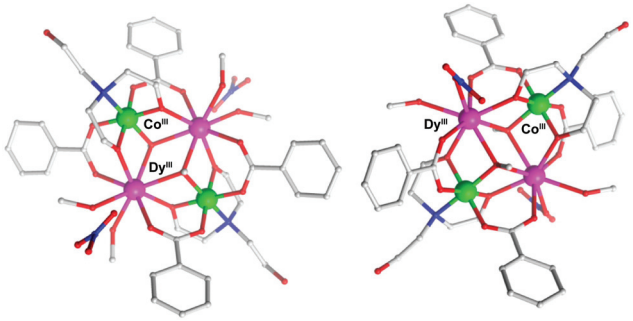

Fig. 16 Structure of $[Co^{III}_2Dy^{III}_2(OMe)_2(teaH)_2(O_2CPh)_4(MeOH)_4](NO_3)_2{\cdot}MeOH{\cdot}H_2O$ (left) and $[Co^{III}_2Ln^{III}_2(OMe)_2(teaH)_2(O_2CPh)_4(MeOH)_2(NO_3)_2]{\cdot}MeOH{\cdot}H_2O$ (right) in the crystal. Reprinted with the permission from ref. 34*a*. Copyright 2015 American Chemical Society.

logues display a field-induced single-ion magnetic behavior at lower temperatures.

III.3.a. Tetranuclear $\{Co^{III}_2Dy^{III}_2\}$ complexes. The most prominent examples of the Co^{III}–Ln^{III} SMM family are the butterfly complexes reported by Murray *et al.*[34] It must be mentioned that a $\{Cr^{III}_2Dy^{III}_2\}$ complex containing paramagnetic 3d and 4f ions revealed a U_{eff} of 55 K.[22a] Analogous Co^{III} complexes $[Co^{III}_2Ln^{III}_2(OMe)_2(teaH)_2(O_2CPh)_4(MeOH)_4](NO_3)_2{\cdot}MeOH{\cdot}H_2O$ {Ln = Gd^{III} Tb^{III}, and Dy^{III}} (Fig. 16) and $[Co^{III}_2Ln^{III}_2(OMe)_2(teaH)_2(O_2CPh)_4(MeOH)_2{\cdot}(NO_3)_2]{\cdot}MeOH{\cdot}H_2O$ {Ln^{III} = Gd^{III}, Tb^{III}, and Dy^{III}} could be prepared.[26d,e,34] The Dy^{III} complex shows SMM behavior with an energy barrier of 62 K and the QTM here is effectively suppressed due to weak magnetic exchange between the Dy(III) ions.[35]

Ab initio calculations reveal that the energy barrier obtained is around 90 K for the complexes $[Co^{III}_2Dy^{III}_2(OMe)_2(teaH)_2(O_2CPh)_4(MeOH)_4](NO_3)_2{\cdot}MeOH{\cdot}H_2O$ and

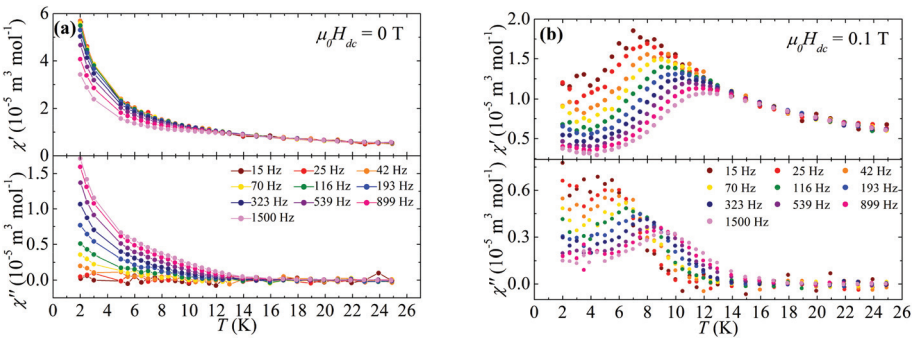

Fig. 15 (a) AC susceptibility *vs.* temperature for **9a** with μ_0H_{dc} = 0 T. (b) AC susceptibility *vs.* temperature for **9a** with μ_0H_{dc} = 0.1 T.[26a] Reprinted with the permission from ref. 26*a*. Copyright 2015 Wiley-VCH.

Table 3 Representative Co^{III}/Ln^{III} complexes (either zero or field induced single-ion magnets) reported in literature, along with their effective energy barrier

Co^{III}/Ln^{III} complex	Energy barrier (U_{eff})	Ref.
$[Co^{III}_2Ln^{III}(L)_2(\mu\text{-}O_2CCH_3)_2(H_2O)_3]{\cdot}NO_3{\cdot}MeOH{\cdot}4H_2O$ (H_3L = 2-methoxy-6-[{2-(2-hydroxyethylamino) ethylimino}methyl]phenol)	88 K	26*a*
$[Co^{III}_2Dy^{III}(valdien)_2(OCH_3)_2(chp)_2]{\cdot}ClO_4{\cdot}5H_2O$, ($H_2$valdien = *N*1,*N*3-bis(3-methoxysalicylidene) diethylenetriamine)	71.4(4.2) K	26*b*
$[Co^{III}_2Dy^{III}_2(OH)_2(bdea)_2(acac)_2(NO_3)_4]$	169 K	26*c*
$[Co^{III}_2Dy_2(L)_2(CH_3CO_2)_4(OH)_2(H_2O)_2]{\cdot}(ClO_4)_2{\cdot}4CH_3CN$ [H_2L = *N*1,*N*3-bis(3-methoxysalicylidene)diethylene triamineligand]	33.8 K	26*d*
$[Co^{III}_2Ln^{III}_2(OMe)_2(teaH)_2(O_2CPh)_4(MeOH)_4](NO_3)_2{\cdot}MeOH{\cdot}H_2O$ [Ln = Tb, Dy], $[Ln^{III}_2Co^{III}_2(OMe)_2(teaH)_2(O_2CPh)_4(MeOH)_2(NO_3)_2]{\cdot}MeOH{\cdot}H_2O$ ($teaH_3$ = triethanolamine)	88.8 K (for Dy analogue), 14.31 K, 18.99 K (for Tb analogue)	26*e*
$[Co^{III}Dy^{III}(OMe)_2(teaH)_2(O_2CPh)_4(MeOH)_4](NO_3)_2{\cdot}MeOH{\cdot}H_2O$, ($teaH_3$ = triethanolamine)	62 K	26*g*
$[Co^{III}_2Dy^{III}_2(OMe)_2(teaH)_2(Piv)_6]$	51 and 127 K	26*h*

$teaH_3$ = triethanolamine, Piv = trimethylacetate

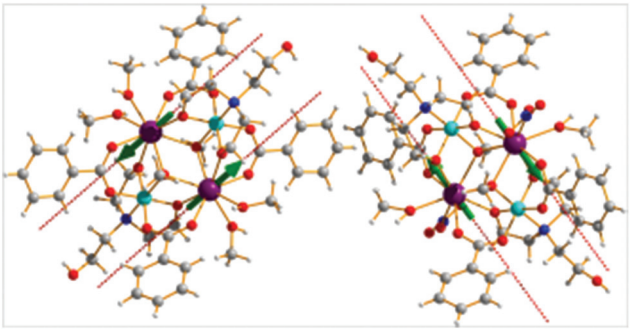

Fig. 17 Orientation of the local magnetic moments in the ground doublet of $[Co^{III}_2Dy^{III}_2(OMe)_2(teaH)_2(O_2CPh)_4(MeOH)_4](NO_3)_2\cdot MeOH\cdot H_2O$ (left) and $[Co^{III}_2Dy^{III}_2(OMe)_2(teaH)_2(O_2CPh)_4(MeOH)_2(NO_3)_2]\cdot MeOH\cdot H_2O$ (right). Green arrows show the antiferromagnetic coupling of the local magnetic moments of the Dy^{III} ions in the ground state. Reprinted with the permission from ref. 34*a*. Copyright 2015 American Chemical Society.

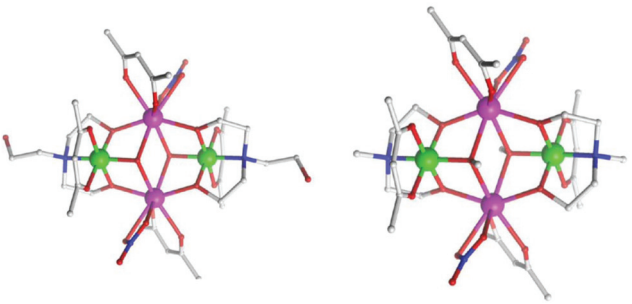

Fig. 18 Molecular structures of **10b** (left) and **10c** (right) that highlight the μ_3-OH (**10b**) and μ_3-OMe (**10c**) bridging ligands and the differing ligand backbones associated with the amine-based polyalcohol ligands. The hydrogen atoms are omitted for clarity. Color scheme: Co^{III}, green; Dy^{III}, purple; O, red; N, blue; C, light gray.[35a] Reprinted with the permission from ref. 35*a*. Copyright 2015 American Chemical Society.

$[Co^{III}_2Dy^{III}_2(OMe)_2(teaH)_2(O_2CPh)_4(MeOH)_2(NO_3)_2]\cdot MeOH\cdot H_2O$ which is in agreement with the single thermally activated relaxation regime (Fig. 17). The orientation of the main anisotropic axis of the ground KD of the individual ions are almost parallel to each other and not differing by more than 4 degrees.[10,35,36]

The exchange part is obtained by fitting the magnetic data to a generalized Lines model.[37a,b] It has been noted that the dipolar coupling is four times that of the exchange coupling having antiferromagnetic type.[13,34b] The splitting of ground exchange doublet is of the order 10^{-6} cm^{-1} implying QTM in each of the cases is significantly weak. This tunneling gap may be due to the non Kramers nature of the coupled state and contribution from the interaction with the transverse field induced by the magnetic moment of the surrounding complexes.[13,31b,36] However, since the ground state is nonmagnetic because of antiferromagnetic intra-cluster exchange, the magnetic field arising from surrounding complexes will diminish with lowering temperature. This is because only the ground (nonmagnetic) state of each molecule remains populated when T approaches 0 K. It is for this reason that the QTM is efficiently suppressed in this unique case.[34a,b]

By modifying the ligand (ligand **10**, Chart 1) another series of butterfly complexes were synthesized: $[Co^{III}_2Dy^{III}_2(OMe)_2(teaH)_2(acac)_4(NO_3)_2]$ (**10a**), $[Co^{III}_2Dy^{III}_2(OH)_2(teaH)_2(acac)_4(NO_3)_2]\cdot 4H_2O$ (**10b**), and $[Co^{III}_2Dy^{III}_2(OMe)_2(mdea)_2$-$(acac)_4(NO_3)_2]$ (**10c**) (Fig. 18). These complexes reveal SMM behavior with thermally activated barriers of 27, 28 and 38 K respectively above 7.5 K (Fig. 19). Table 3 summarizes representative examples of Co^{III}/Ln^{III} complexes.

Utilizing *o*-toluic acid (**11**) as the ligand the complexes $[Co^{III}_2Ln^{III}_2(\mu_3\text{-}OH)_2(o\text{-}tol)_4(mdea)_2(NO_3)_2]$ (mdea = *N*-methyldiethanolamine) (Ln = Dy (**11a**), Tb (**11b**), Ho (**11c**)) (Fig. 20), were synthesized and characterized.[38a] In the absence of magnetic field complex **11a** shows SMM behavior with an energy barrier of 81.2 K whereas complexes **11b** and **11c** show field-induced SMM properties (Fig. 21 and 22).[38a] The effect of diamagnetic metal ion in influencing the barrier height is explored in detail through model complexes where the diamagnetic Co^{III} ion is replaced with K^I, Zn^{II}, and Ti^{IV} leading to $\{K_2Dy^{III}_2\}$ (model **11e**), $\{Zn^{II}_2Dy^{III}_2\}$ (model **11f**), and $\{Ti^{IV}_2Dy^{III}_2\}$ (model **11g**).[23c]

Calculations yield barrier heights of 88.8 K, 358 K, 127 K and 48 K for **11a**, **11e–11g** respectively and these values

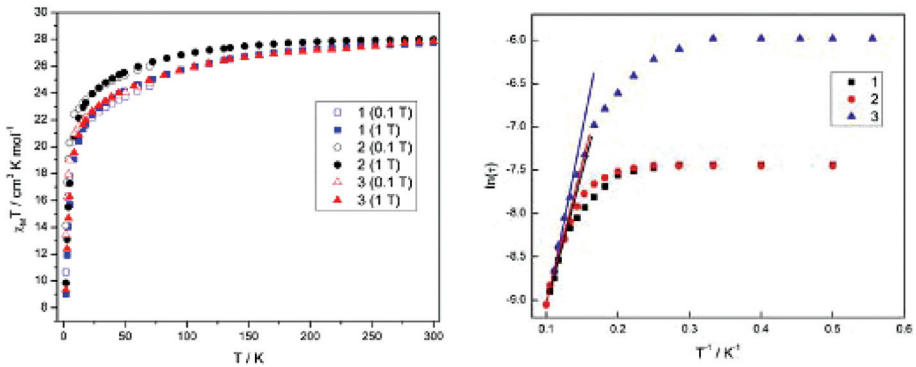

Fig. 19 χT *vs.* T and relaxation time τ *vs.* T for complex **10a**, **10b** and **10c**. Reprinted with the permission from ref. 35*a*. Copyright 2015 American Chemical Society.

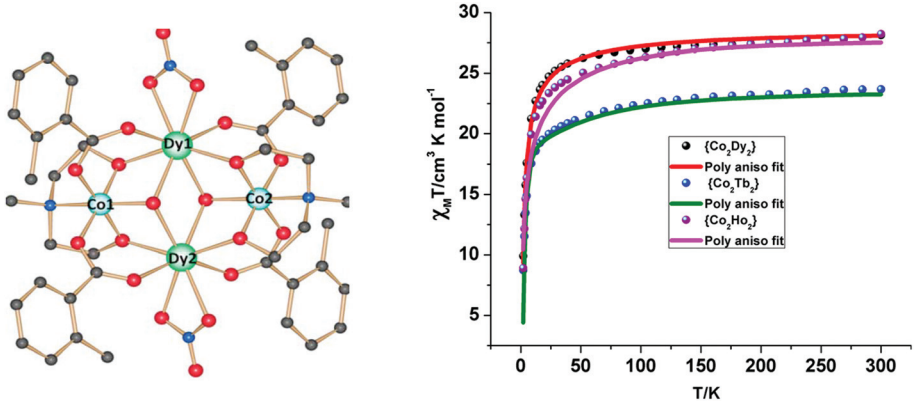

Fig. 20 Molecular structure of **11a** and plots of χT *versus* T plots for **11a–11c** (dotted line). The solid lines are fits of the data using the Lines model employing the POLY_ANISO program.[38a] Reprinted with the permission from ref. 38*a*. Copyright 2017 American Chemical Society.

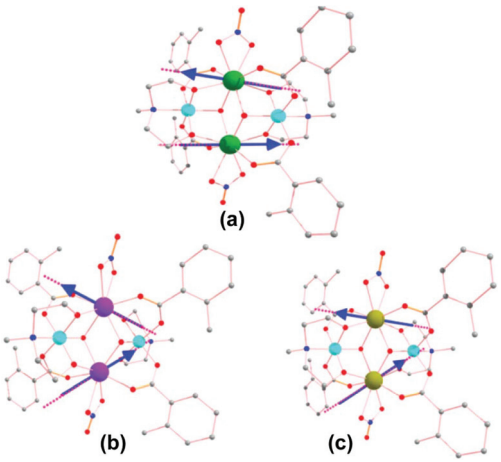

Fig. 21 Orientations of the local magnetic moments in the ground doublet of complexes (a) **11a**, (b) **11b**, and (c) **11c**. Blue arrows show the anti-ferromagnetic coupling of the local magnetic moments of the Ln^{III} ions in the ground state. Reprinted with the permission from ref. 38*a*. Copyright 2017 American Chemical Society.

suggest that the inclusion of diamagnetic ion increases the effective energy barrier in these complexes (Fig. 23). The relaxation mechanism developed reveal that the presence of the diamagnetic ion also quenches the QTM probabilities due to enhanced axial interaction as desired for an oblate Dy^{III} ion (Fig. 24).[34a,b]

For the complex **11**, the ground KDs are purely of the Ising type with very small transverse components of (g_x = 0.0002, g_y = 0.0003, and g_z = 19.9797 for Dy1 and g_x = 0.0002, g_y = 0.0003, and g_z = 19.9124 for Dy2) which is in contrast to the model complex **11d** where no diamagnetic ion is present. The QTM is reduced here and the energy barrier is also increased to 358.9 cm^{-1} for Dy1 and 359.8 cm^{-1} for Dy2 (**11e**). Similar effect has been observed also for two other diamagnetic ions, namely Zn^{II} and Ti^{IV}. This enhancement can be attributed to the fact that the closed shell M^{II} ion offers a stronger electrostatic repulsion, resulting in a greater negative charge on O and thus favors a stronger axiality (Fig. 25).[38a]

III.3.b. Hetero metallic octanuclear [TM$^{III}_4$Dy$^{III}_4$] (TM = Co^{III} *vs.* Cr^{III}) SMMs. Four complexes, [Co$^{III}_4$Dy$^{III}_4$(μ-OH)4(μ$_3$-

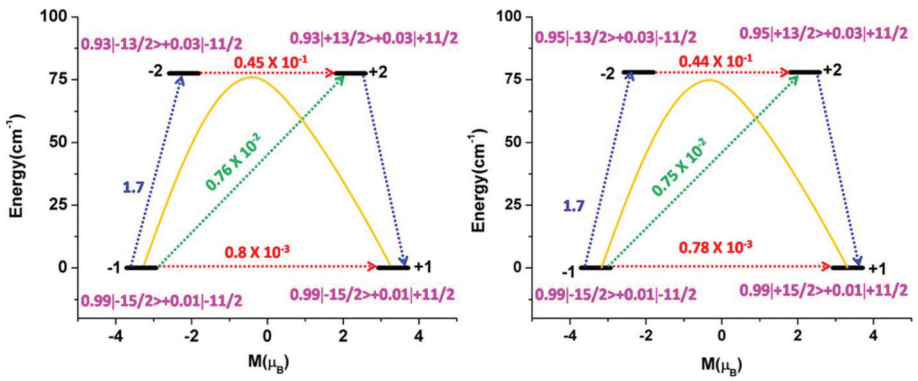

Fig. 22 Magnetization blocking barrier for (left) the Dy1 site (right) and the Dy2 site in **11a** computed *ab initio*. The thick black line indicates the Kramers doublets (KDs) as a function of computed magnetic moment. The green/blue arrows show the possible pathway through Orbach/Raman relaxation. The dotted red lines represent the presence of QTM/TA-QTM between the connecting pairs. The numbers provided at each arrow are the mean absolute values for the corresponding matrix element of the transition magnetic moment. The yellow curve indicates the most possible relaxation pathway.[38a] Reprinted with the permission from ref. 38*a*. Copyright 2017 American Chemical Society.

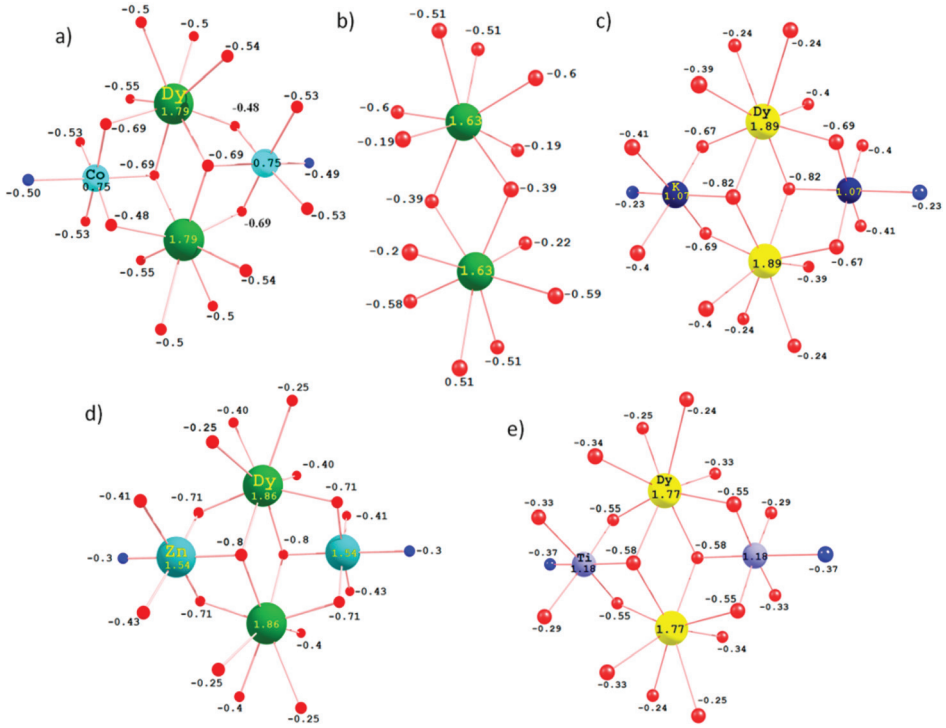

Fig. 23 DFT computed Mulliken charges on the donor atoms of complexes (a) **11a**, (b) **11d**, (c) **11e**, (d) **11f**, and (e) **11g**. Reprinted with the permission from ref. 38*a*. Copyright 2017 American Chemical Society.

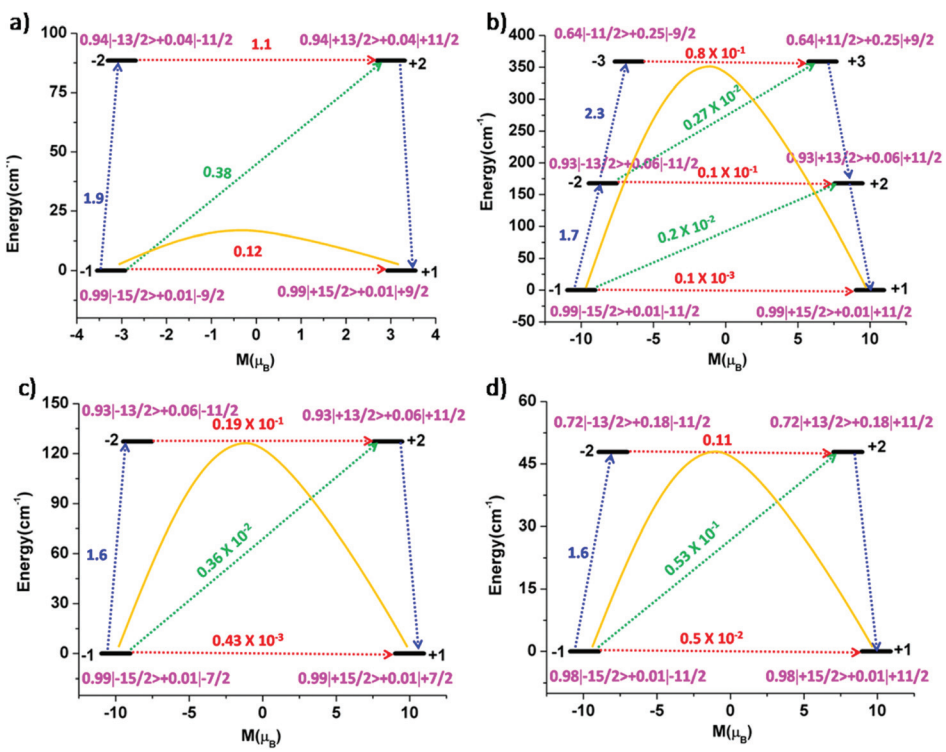

Fig. 24 Magnetization blocking barrier for the Dy1 site in (a) **11d**, (b) **11e**, (c) **11f**, and (d) **11h**. The thick black line indicates the Kramers doublets (KDs) as a function of computed magnetic moment. The green/blue arrows show the possible pathway through Orbach/Raman relaxation. The dotted red lines represent the presence of QTM/TA-QTM between the connecting pairs. The numbers provided at each arrow are the mean absolute values for the corresponding matrix element of the transition magnetic moment. Reprinted with the permission from ref. 38*a*. Copyright 2017 AmericanChemical Society.

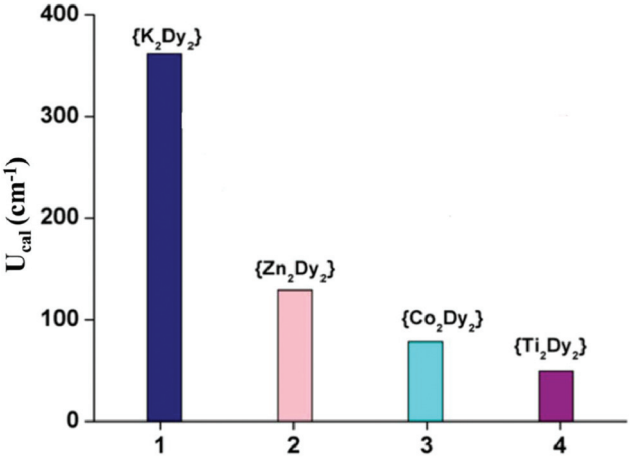

Fig. 25 Comparison of U_{cal} value computed for models **11e**, **11f**, **11a** and **11g** using *ab initio* calculations. Reprinted with the permission from ref. 38*a*. Copyright 2017 American Chemical Society.

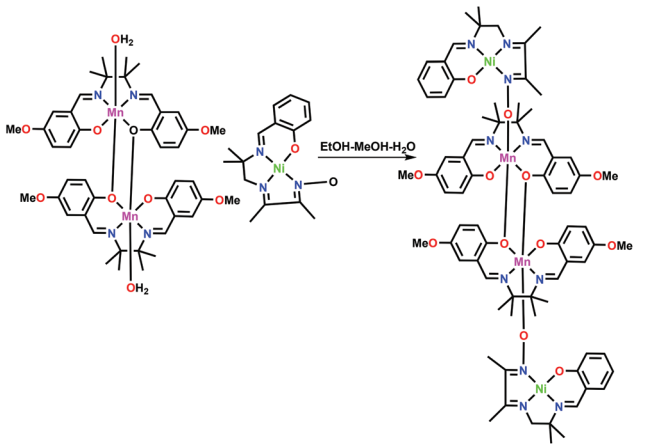

Scheme 7 Synthesis of heterometallic $Ni^{II}_2Mn^{III}_2$ where Ni^{II} is in square planar geometry.[27a]

OMe)$_4${O$_2$CC(CH$_3$)$_3$}$_4$(tea)$_4$(H$_2$O)$_4$]·4H$_2$O (**10i**), [$Co^{III}_4Dy^{III}_4$(μ-F)$_4$(μ$_3$-OH)$_4$(*o*-tol)$_8$(mdea)$_4$]·3H$_2$O·EtOH·MeOH (**10j**; tea3$^-$ = triply deprotonated triethanolamine; mdea^{2-} = doubly deprotonated *N*-methyldiethanolamine; *o*-tol = *o*-toluate), [$Cr^{III}_4Dy^{III}_4$(μ-F4)(μ$_3$-OMe)$_{1.25}$(μ$_3$-OH)$_{2.75}$(O$_2$CPh)$_8$(mdea)$_4$] (**10k**) and [$Cr^{III}_4Dy^{III}_4$(μ$_3$-OH)$_4$(μ-N$_3$)$_4$(mdea)$_4$(O$_2$CC(CH$_3$)$_3$)$_4$] (**10l**) were prepared and characterized (Fig. 26).[38b] All the four complexes have same structural topology. It is easy to compare the ligand field substitution and the effect of transition metal ion in this series. Complexes **10j**, **10k** and **10l** exhibited slow magnetic relaxation with barrier heights (U_{eff}) of 39.0 K, 55.0 K and

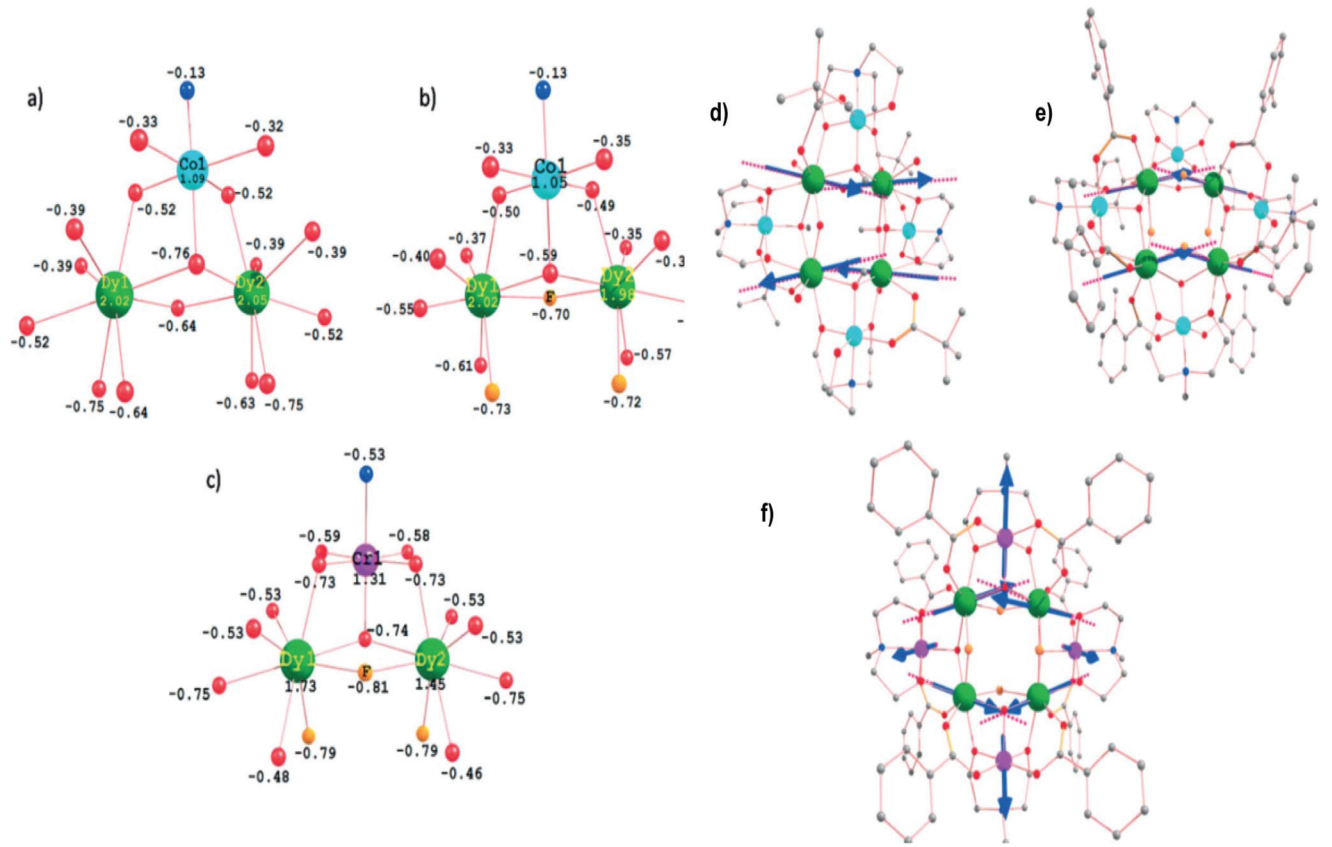

Fig. 26 DFT computed Mulliken charges on the donor atoms of **10i** for (a) and (d); **10j** for (b) and (e); **10k** for (c) and (f). Reprinted with the permission from ref. 38*b* Copyright 2017 Wiley-VCH.

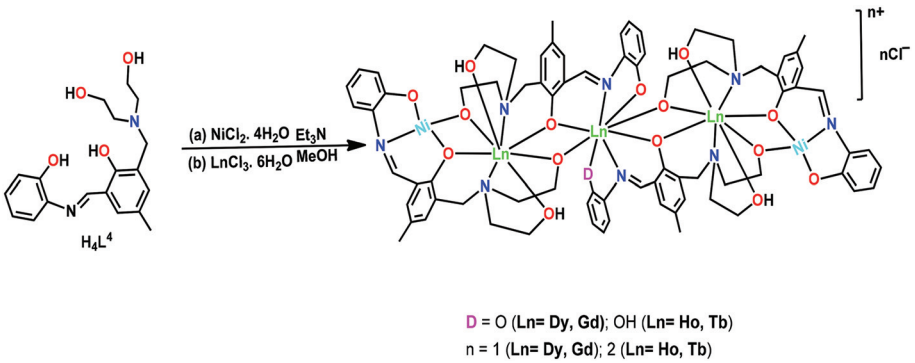

Scheme 8 Synthesis of pentanuclear $Ni^{II}_2Ln^{III}_3$ complexes.[27c]

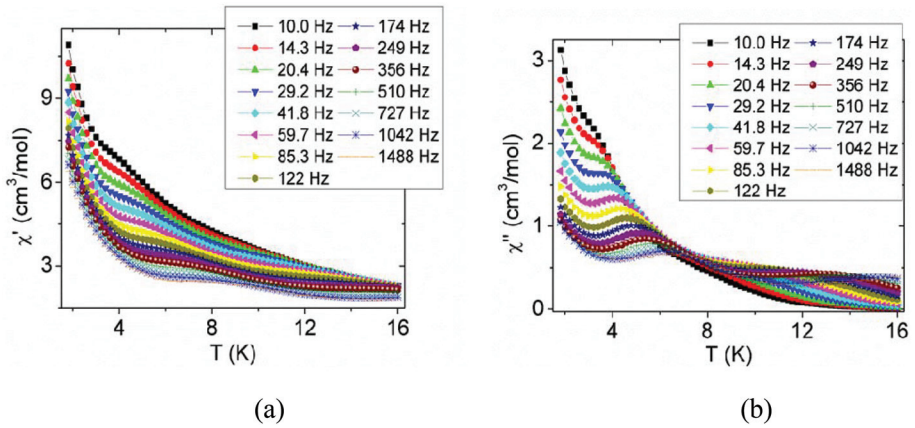

Fig. 27 (a) In phase signal of an ac measurement of $Ni^{II}_2Dy^{III}_3$ and (b) out of phase signal of the same measurements of $Ni^{II}_2Dy^{III}_3$.[27c] Reprinted with the permission from ref. 27*c*. Copyright 2013 American Chemical Society.

10.4 K respectively. Here unlike earlier examples, where diamagnetic ions were found to enhance the barrier height, the molecules containing Cr^{III} ion are found to be superior. This is essentially due to weak $Ln^{III}\cdots Ln^{III}$ exchange that results in stronger QTM at the ground state. A paramagnetic ion with stronger coupling quenches the tunneling probability leading to better SMM characteristics. Despite the fact that the diamagnetic Co^{III} ion improves the single-ion magnetic properties, in this topology the presence of a diamagnetic ion is found to be disadvantageous. Thus, the choice of metal ion and the structural topology are the most important parameters that can dictate the magnetic properties.[29b]

III.4. Heterometallic complexes with square planar Ni^{II} ($S = 0$)

Heterometallic 3d/4f complexes containing diamagnetic Ni^{II} (low spin, square planar geometry) are rare. An example of this is illustrated in Scheme 7.[27a] Usually, Ni^{II} (d^8) ion is paramagnetic in both octahedral ($t_{2g}^6e_g^2$) and tetrahedral ($e^4t_2^4$) geometries and not very anisotropic in octahedral systems, but shows interesting anisotropy in tetrahedral systems.[15c] We felt that the combination of square planar Ni^{II}–Ln^{III} complexes should be interesting. For this purpose we designed the ligand H_4L (**12**) (Chart 1) which contains four cluster propagating –OH groups. Accordingly, the reaction of **12** with $Ln^{III}Cl_3{\cdot}6H_2O$ and $Ni^{II}Cl_2{\cdot}4H_2O$ salts in the presence of NEt_3, afforded isostructural pentanuclear heterometallic complexes[27c] (Scheme 8), $[Ni^{II}_2Dy^{III}_3(LH)_4]{\cdot}Cl$ (**12a**), $[Ni_2Gd_3(LH)_4]{\cdot}Cl$ (**12b**), $[Ni^{II}_2Tb^{III}_3(LH)_3(LH_2)]{\cdot}Cl_2$ (**12c**), $[Ni^{II}_2\ Ho^{III}_3\ (LH)_3\ (LH_2)]{\cdot}Cl_2$ (**12d**). In all these complexes Ni^{II} possesses a square planar geometry. Among the three lanthanide ions the two terminal lanthanide ions are in a distorted trigonal-dodecahedron geometry while the central lanthanide ion possesses a distorted square antiprism geometry.

Magnetic measurements indicate that the complex {**12a**} possesses significant magnetic anisotropy and the variable

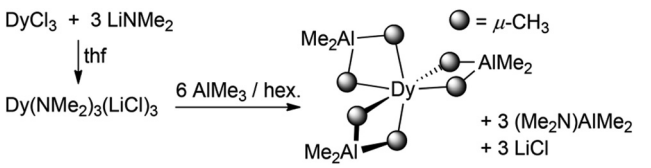

Scheme 9 Reaction scheme for preparation of complex, $[Dy^{III}(Al^{III}Me_4)_3]$.[14a] Adopted from ref. 14*a*. Reproduced by permission of The Royal Society of Chemistry.

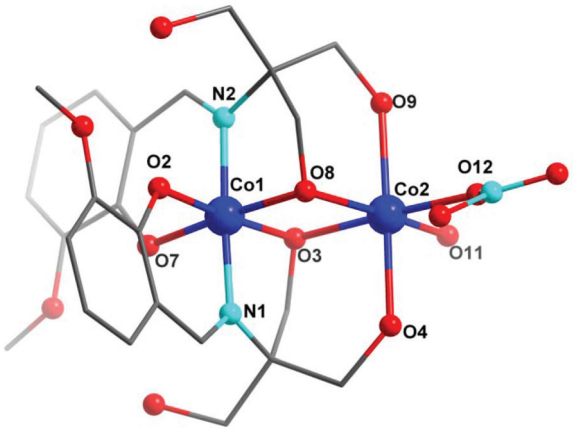

Fig. 28 Molecular structure of (Co^{II}–Co^{III})–NO_3 (**13c**).[39c] Reprinted with the permission from ref. 39c. Copyright 2013 American Chemical Society.

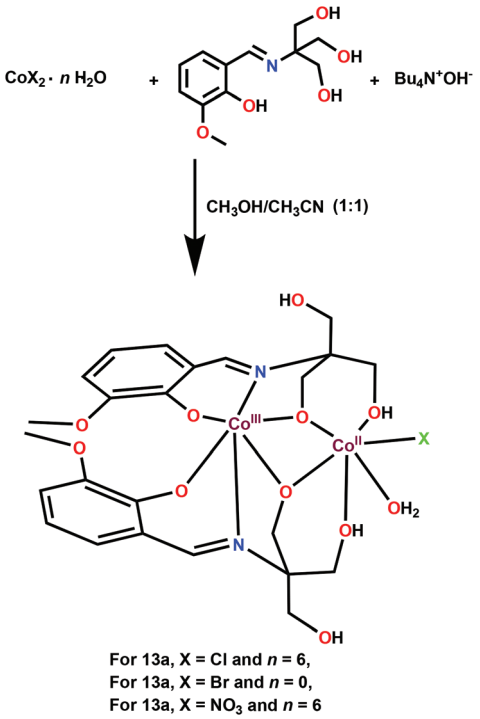

Scheme 10 Synthesis of mixed valent Co^{III}–Co^{II} complexes **13a–c**.[39c]

temperature and variable frequency ac susceptibility measurements reveal that **12a** shows a typical SMM behavior with at least two relaxation processes (Fig. 27). Two relaxation processes with the characteristics, U_{eff} = 85 K and $\tau_0 = 5.9 \times 10^{-7}$ s (high temperature), and U_{eff} = 53.5 K, $\tau_0 = 2.3 \times 10^{-8}$ s (low temperature) are seen and are probably due to two geometrically different lanthanide ions in the complex. Arrhenius plot extracted from the ac susceptibility data leads to a value of 85 K for the effective energy barrier (Fig. 27). Further magnetic measurement studies revealed an open hysteresis loop up to 3 K for **12a** at sweep rates faster than 50 mT s^{-1}.

III.5. Heterometallic complexes with Al^{III} ions

Another interesting diamagnetic substitution effect was analyzed by considering a Al^{III} linked to Dy^{III} in a octahedral fashion in $[Dy^{III}(Al^{III}Me_4)_3]$ (Scheme 9).

The Dy^{III} ion in $[Dy^{III}(Al^{III}Me_4)_3]$ is present in a distorted octahedral arrangement. The *ab initio* studies shows that the *g*-tensors in the ground doublets in $[Dy^{III}(Al^{III}Me_4)_3]$ (g_x = 0.10, g_y = 3.04, g_z = 15.73) are strongly axial, but they both depart significantly from the Ising limit with a large contribution towards the transverse anisotropy.[31b,36] The orientation of the magnetic moment does not coincide with the three fold symmetry axis of the complex. The principal axis of the first excited KD also deviates significantly from the ground KD (38.7 degree). The lack of uniaxiality and significant transverse anisotropies causes the energy barrier between the ground and first excited state to be 10.9 cm^{-1} making this complex a poor SMM. A diluted complex of the above with Y^{III} (In 20 : 1 ratio to Dy^{III}) revealed a slow relaxation, under an applied field, below 3 K.[13]

IV. Homometallic Co^{II}/Co^{III} complexes[39]

Although not directly related to the theme of 3d/4f complexes or 3p/4f complexes, we describe a mixed valent dinuclear Co^{II}/Co^{III} complex since in this instance also the magnetic pro-

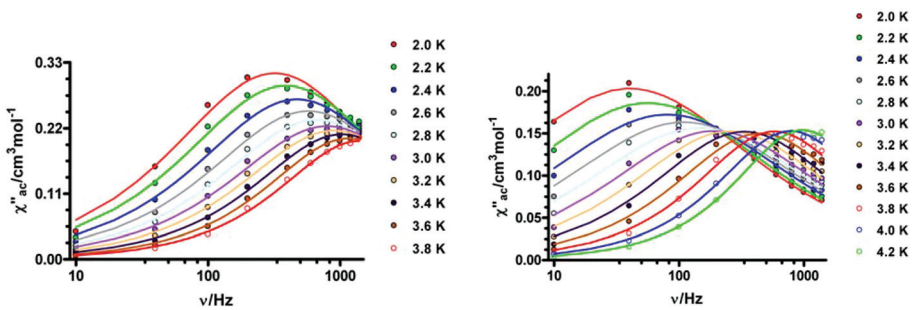

Fig. 29 AC susceptibility measurement of the mixed valent complexes, **13a** and **13b**. Reprinted with the permission from ref. 39c. Copyright 2013 American Chemical Society.

Table 4 Some reported Co^{II}–Co^{III} based SMMs[a]

Compound	Energy Barrier, U_{eff} (H_{dc}) Pre-exponential factor (τ_0/s)	Ref.
$[H(NEt_3)]^+[Co^{II}Co^{III}_3(L^1{}_R)_6]^-$ (2R)	38 K (0), $\tau_0 = 8.3 \times 10^{-7}$ 41 K (1500 Oe), $\tau_0 = 6.4 \times 10^{-7}$	39*a*
$[H(DBU)]^+[Co^{II}Co^{III}_3(L^1{}_R)_6]^-$ (3R)	52 K (0), $\tau_0 = 5.0 \times 10^{-7}$ 54 K (1500 Oe), $\tau_0 = 2.8 \times 10^{-7}$	39*a*
$[H(NEt_3)]^+[Co^{II}Co^{III}_3(L^2{}_R)_6]^-$ (4R)	43 K (0), $\tau_0 = 2.0 \times 10^{-7}$ 45 K (1500 Oe), $\tau_0 = 2.4 \times 10^{-7}$	39*a*
$[H(DBU)]^+[Co^{II}Co^{III}_3(L^3{}_R)_6]^-$ (5R)	127 K (0), $\tau_0 = 5.8 \times 10^{-8}$ 130 K (1500), $\tau_0 = 5.4 \times 10^{-8}$	39*a*
$[H(DIPEA)]^+[Co^{II}Co^{III}_3(L^4{}_R)_6]^-$ (6R)	129 K (0), $\tau_0 = 5.7 \times 10^{-8}$ 134 K (1500 Oe), $\tau_0 = 4.5 \times 10^{-8}$	39*a*
$[H(DBU)]^+[Co^{II}Co^{III}_3(L^4{}_R)_6]^-$ (7R)	137 K (0), $\tau_0 = 5.3 \times 10^{-8}$ 139 K (1500 Oe), $\tau_0 = 4.6 \times 10^{-8}$	39*a*
$(n\text{-}Bu_4N)^+[Co^{II}Co^{III}_3(L^4{}_R)_6]^-$ (8R)	147 K (0), $\tau_0 = 2.5 \times 10^{-8}$ 162 K (1500 Oe), $\tau_0 = 1.2 \times 10^{-8}$	39*a*
$[Co^{II}Co^{III}_4(piv)_4(teaH)_2(bicH)_2(OH)_2]\cdot 4H_2O\cdot CH_3CN$	25 K (1400 Oe) $\tau_0 = 6.0 \times 10^{-7}$ $U_{eff} = 27\ cm^{-1}$ (2600 Oe) $\tau_0 = 3.5 \times 10^{-7}$	39*b*
$[Co^{II}_4Co^{III}_3(HL)_6(NO_3)_3(H_2O)_3][NO_3]_2$ {$H_3L = H_2NC(CH_2OH)_3$ = 2-amino-2-(hydroxymethyl) propane-1,3-diol or 'tris'}	Below 4 K, frequency dependent out-of-phase ac signal is observed	39*d*

[a] Ligands, utilized for the preparation of complexes detailed in this table are given in Chart 3.

perties are due to a paramagnetic ion that is linked with a diamagnetic ion. The molecular structure of this mixed valent complex is shown in Fig. 28.[39c] Interestingly, the Co^{II} is bound, apart from other ligands, by a Cl/Br/NO_3 group (Scheme 10). By changing this coordinating group the magnetic properties can be fine-tuned. AC susceptibility measurements reveals that slow relaxation of magnetization is observed for two complexes containing Cl/Br as coordinating group [$\tau_0 = 6.1 \times 10^{-6}$ s for (Co^{II}–Co^{III})–Cl (**13a**) complex; $\tau_0 = 1.0 \times 10^{-6}$ s for (Co^{II}–Co^{III})–Br complex (**13b**)] (Fig. 29). Comparison with other reported Co^{II}–Co^{III} complexes is given in Table 4.

V. Conclusions

In this perspective, we have discussed how diamagnetic ions can be utilized to enhance the magnetic properties of 3d/4f complexes where the 3d metal ion is diamagnetic. We have discussed some related examples where instead of a 3d diamagnetic metal ion, other diamagnetic metal ions are present. The lessons learnt from this study can be summarized as follows.

(i) In lanthanide based SIMs, the diamagnetic ions which are directly connected to the lanthanide ion by bridging ligands, tend to offer an advantage by polarizing the bridging atom and thus enhancing the charge on the ligand atom which in turn offer stronger interaction to the lanthanide ions. This enhanced interaction with the lanthanide is found to (a) enhance the ground-state-excited state gap (b) reduce the mixing of wave function and hence reduce the QTM probability and hence leads to better SMM characteristics. Additionally, the presence of the diamagnetic metal ions results in an effective *internal dilution* and causes a reduction in the intermolecular interaction, the latter being one of the causes of QTM in many instances.

(ii) Several diamagnetic ions were found to influence the magnetic properties and the very first examples considered were {$Mg^{II}_2Dy^{III}$} (**2d**) and {$Zn^{II}_2Ln^{III}$} (**2a**) complexes where the former is found to be have larger U_{eff} than the latter. This suggests that Mg^{II} cation is slightly superior compared to Zn^{II} cation in offering grater axiality for the anisotropy as they are found to lie along the g_{zz} direction.

(iii) In the next example, we have looked into the iso-structural complexes of Dy^{III}HL (**3a**) and $Zn^{II}Dy^{III}$HL (**4a**) to unveil how Zn^{II} substitution leads to five-fold increase in the energy barrier. Combined DFT and *ab initio* calculations clearly reveals that the bridging oxygen accumulates greater negative charge due to strong polarization by the Zn^{II} ion leading to larger gap in m_J levels and quenching of QTM effects. Additionally, increasing the number of Zn^{II} ions in conjunction with Dy^{III} ion has proven to be beneficial. Particularly, complexes having a linear Zn^{II}–Dy^{III}–Zn^{II} motif are found to offer polarization on atoms on both directions leading to higher barriers. However a similar effect on a prolate Er^{III} ion found to be counterproductive as Zn^{II} ions does not lie in the desired direction.

(iv) Any secondary coordination effect which would otherwise influence the electron density around Zn^{II} is also found to influence the magnetic properties of Dy^{III} ion. For examples varying the counter ions such as PF_6, ClO_4 found to have pronounced effect on Zn^{II} substitution than the CH_3OH analogue. Also, if Zn^{II} ions are included in the formation of larger Ln cluster aggregation, other benefits are noticeable.

Incorporation of three Zn^{II} ion in the cluster formation of a $\{Dy_3^{III}\}$ triangle reveal that the presence of Zn^{II} ion enforce the g_{zz} axis to lie within the triangular plane leading to the observation of toroidic behavior.

(v) Apart from Zn^{II} ions, other diamagnetic ions also have greater impact and the well-studied cation in this category includes Co^{III} ion. In particular, $\{Co_2^{III}Ln_2^{III}\}$ butterfly complexes[26i,j] have been studied extensively by Murray and co-workers which affirm enhancement of the energy barrier due to diamagnetic metal ion *via* quenching of QTM process. *Ab initio* calculations performed on some of the selected systems where Co^{III} ion is replaced by K^{I}, Zn^{II} and Ti^{IV} suggest that enhancement of barrier height with K^{I} exhibiting the largest barrier among the studied model systems. A similar effect is noticeable also for higher nuclearity clusters such as $\{Dy_4^{III}Co_4^{III}\}$.

(vi) Incorporation of square planar Ni^{II} with $S = 0$ ground state in 3d–4f molecules is found to lead to SMM characteristics. There are a few examples with Al^{III} also where the magnetic properties can be altered by the inclusion of Al^{III} ion.

(vii) Additionally, diamagnetic substitution effects are noticeable beyond lanthanides. Thus, mixed-valent Co^{II}/Co^{III} complexes exhibit appealing magnetic properties due to the diamagnetic Co^{III} cation.

In summary, it is clear that the diamagnetic ions help to enhance the effective energy barriers in many cases, if placed suitably in the coordination sphere of the lanthanide ions. In particular, the polarizing ability of such ions seems to play an important role. However, these studies involving the role of diamagnetic metal ions are still quite limited in comparison to the large volume of literature in the field of SMMs and SIMs. Hopefully, the knowledge gained thus far in this new paradigm, will allow a further blossoming of this area.

Conflicts of interest

There are no conflicts to declare.

Acknowledgements

V. C. is thankful to the Department of Science and Technology, New Delhi, India, for a National J. C. Bose Fellowship. A. C. is thankful to Tata Institute of Fundamental Research, Hyderabad and SERB-National Postdoctoral Fellowship (PDF/2015/000622). P. K. and J. G. are thankful to the National Institute of Science Education and Research, Bhubaneswar, for doctoral and post-doctoral fellowship respectively. G. R. would like to thank the SERB (EMR/2014/00024) and INSA for funding.

References

1 (*a*) G. Christou, D. Gatteschi, D. N. Hendrickson and R. Sessoli, *MRS Bull.*, 2000, **25**, 66–71; (*b*) J. Cirera, E. Ruiz, S. Alvarez, F. Neese and J. Kortus, *Chem. – Eur. J.*, 2009, **15**, 4078–4087; (*c*) M. Nakano and H. Oshio, *Chem. Soc. Rev.*, 2011, **40**, 3239–3248; (*d*) M. Murugesu, *Nat. Chem.*, 2012, **4**, 347–363; (*e*) R. Sessoli, H.-L. Tsai, A. R. Schake, S. Wang, J. B. Vincent, K. Folting, D. Gatteschi, G. Christou and D. N. Hendrickson, *J. Am. Chem. Soc.*, 1993, **115**, 1804–1816.

2 M. Andruh, *Dalton Trans.*, 2015, **44**, 16633–16653.

3 (*a*) L. Bogani and W. Wernsdorfer, *Nat. Mater.*, 2008, **7**, 179–186; (*b*) M. N. Leuenberger and D. Loss, *Nature*, 2001, **410**, 789–793.

4 (*a*) T. Feder, *Phys. Today*, 2001, **62**, 21; (*b*) Y.-Z. Zheng, G.-J. Zhou, Z. Zheng and R. E. P. Winpenny, *Chem. Soc. Rev.*, 2014, **43**, 1462–1475; (*c*) V. K. Pecharsky and K. A. Gschneidner Jr., *J. Magn. Magn. Mater.*, 1999, **200**, 44–56.

5 (*a*) T. Filippo and M. Affronte, *Chem. Soc. Rev.*, 2011, **40**, 3119–3129; (*b*) M.-H. Jo, J. E. Grose, K. Baheti, M. M. Deshmukh, J. J. Sokol, E. M. Rumberger, D. N. Hendrickson, J. R. Long, H. Park and D. C. Ralph, *Nano Lett.*, 2006, **6**, 2014–2020.

6 (*a*) R. E. P. Winpenny, *Angew. Chem., Int. Ed.*, 2008, **47**, 7992–7994; (*b*) M. N. Leuenberger and D. Loss, *Nature*, 2001, **410**, 789–793.

7 (*a*) D. Gatteschi and R. Sessoli, *Angew. Chem., Int. Ed.*, 2003, **42**, 268–297; (*b*) E. del Barco, A. D. Kent, S. Hill, J. M. North, N. S. Dalal, E. M. Rumberger, D. N. Hendrickson, N. E. Chakov and G. Christou, *J. Low Temp. Phys.*, 2005, **140**, 119–174; (*c*) P. C. E. Stamp, *Nature*, 1996, **383**, 125.

8 (*a*) W. Wernsdorfer, N. E. Chakov and G. Christou, *Phys. Rev. Lett.*, 2005, **95**, 37203–37204; (*b*) W. Wernsdorfer and R. Sessoli, *Science*, 1999, **284**, 133.

9 (*a*) L. Lecren, W. Wernsdorfer, Y.-G. Li, A. Vindigni, H. Miyasaka and R. Clérac, *J. Am. Chem. Soc.*, 2007, **129**, 5045; (*b*) L. Lecren, O. Roubeau, C. Coulon, Y.-G. Li, X. F. L. Goff, W. Wernsdorfer, H. Miyasaka and R. Clérac, *J. Am. Chem. Soc.*, 2005, **127**, 17353; (*c*) W. Wernsdorfer, M. Soler, G. Christou and D. N. Hendrickson, *J. Appl. Phys.*, 2002, **91**, 7164.

10 (*a*) K. Liua, W. Shi and P. Chenga, *Coord. Chem. Rev.*, 2015, **289–290**, 74–122; (*b*) L. R. Piquer and E. C. Sañudo, *Dalton Trans.*, 2015, **44**, 8771–8780; (*c*) J.-L. Liu, J.-Y. Wu, Y.-C. Chen, V. Mereacre, A. K. Powell, L. Ungur, L. F. Chibotaru, X.-M. Chen and M.-L. Tong, *Angew. Chem., Int. Ed.*, 2014, **53**, 12966–12970.

11 (*a*) S. T. Liddle and J. V. Slageren, *Chem. Soc. Rev.*, 2015, **44**, 6655–6669; (*b*) D. N. Woodruff, R. E. P. Winpenny and R. A. Layfield, *Chem. Rev.*, 2013, **113**, 5110–5148.

12 (*a*) C. A. P. Goodwin, F. Ortu, D. Reta, N. F. Chilton and D. P. Mills, *Nature*, 2017, **548**, 439–442; (*b*) F.-S. Guo, B. M. Day, Y.-C. Chen, M.-L. Tong, A. Mansikkamäki and R. A. Layfield, *Angew. Chem., Int. Ed.*, 2017, **56**, 11445–11449.

13 S. K. Gupta, T. Rajeshkumar, G. Rajaraman and R. Murugavel, *Chem. Sci.*, 2016, **7**, 5181–5191.

14 (*a*) S. N. König, N. F. Chilton, C. M. Mössmer, E. M. Pineda, T. Pugh, R. Anwander and R. A. Layfield, *Dalton Trans.*, 2014, **43**, 3035–3038; (*b*) J. L. Krinsky, S. G. Minasian and J. Arnold, *Inorg. Chem.*, 2011, **50**, 345–357.

15 (*a*) C. Papatriantafyllopoulou, E. E. Moushi, G. Christou and A. J. Tasiopoulos, *Chem. Soc. Rev.*, 2016, **45**, 1597–1628; (*b*) G. A. Craig and M. Murrie, *Chem. Soc. Rev.*, 2015, **44**, 2135–2147; (*c*) S.-D. Jiang, D. Maganas, N. Levesanos, E. Ferentinos, S. Haas, K. Thirunavukkuarasu, J. Krzystek, M. Dressel, L. Bogani, F. Neese and P. Kyritsis, *J. Am. Chem. Soc.*, 2015, **137**, 12923–12928.

16 (*a*) C. M. Zaleski, J. W. Kampf, T. Mallah, M. L. Kirk and V. L. Pecoraro, *Inorg. Chem.*, 2007, **46**, 1954–1956; (*b*) G. Mezei, C. M. Zaleski and V. L. Pecoraro, *Chem. Rev.*, 2007, **107**, 4933.

17 (*a*) R. Sessoli, D. Gatteschi and D. Villain, *J. Molecular Nanomagnets*, Oxford University Press, Oxford, 2006; (*b*) O. Kahn, *Molecular Magnetism*, VCH, New York, 1993.

18 Y.-N. Guo, G.-F. Xu, Y. Guo and J. Tang, *Dalton Trans.*, 2011, **40**, 9953–9963.

19 S. Osa, T. Kido, N. Matsumoto, N. Re, A. Pochaba and J. Mrozinski, *J. Am. Chem. Soc.*, 2004, **126**, 420–421.

20 Co/Gd: V. Chandrasekhar, B. M. Pandian, R. Azhakar, J. J. Vittal and R. Clérac, *Inorg. Chem.*, 2007, **46**, 5140–5142.

21 (*a*) V. Chandrasekhar, P. Bag, M. Speldrich, J. V. Leusen and P. Kögerler, *Inorg. Chem.*, 2013, **52**, 5035–5044; (*b*) V. Chandrasekhar, A. Dey, S. Das, M. Rouzières and R. Clérac, *Inorg. Chem.*, 2013, **52**, 2588–2598; (*c*) P. Bag, A. Chakraborty, G. Rogez and V. Chandrasekhar, *Inorg. Chem.*, 2014, **53**, 6524–6533; (*d*) V. Chandrasekhar, B. M. Pandian, J. J. Vittal and R. Clérac, *Inorg. Chem.*, 2009, **48**, 1148–1157; (*e*) A. Chakraborty, P. Bag, E. Rivière, T. Mallah and V. Chandrasekhar, *Dalton Trans.*, 2014, **43**, 8921–8932.

22 (*a*) J. Rinck, G. Novitchi, W. Van den Heuvel, L. Ungur, Y. Lan, W. Wernsdorfer, C. E. Anson, L. F. Chibotaru and A. K. Powell, *Angew. Chem., Int. Ed.*, 2010, **49**, 7583–7587; (*b*) M. Hołyńska, D. Premužić, I.-R. Jeon, W. Wernsdorfer, R. Clérac and S. Dehnen, *Chem. – Eur. J.*, 2011, **17**, 9605–9610; (*c*) S. Schmidt, D. Prodius, V. Mereacre, G. E. Kostakis and A. K. Powell, *Chem. Commun.*, 2013, **49**, 1696–1698; (*d*) K. C. Mondal, A. Sundt, Y. Lan, G. E. Kostakis, O. Waldmann, L. Ungur, L. F. Chibotaru, C. E. Anson and A. K. Powell, *Angew. Chem., Int. Ed.*, 2012, **51**, 7550–7554; (*e*) F.-H. Zhao, H. Li, Y.-X. Che, J.-M. Zheng, V. Vieru, L. F. Chibotaru, F. Grandjean and G. J. Long, *Inorg. Chem.*, 2014, **53**, 9785–9789; (*f*) F. Mori, T. Nyui, T. Ishida, T. Nogami, K.-Y. Choi and H. Nojiri, *J. Am. Chem. Soc.*, 2006, **128**, 1440–1449.

23 (*a*) J. Ruiz, G. Lorusso, M. Evangelisti, E. K. Brechin, S. J. A. Pope and E. Colacio, *Inorg. Chem.*, 2014, **53**, 3586–3594; (*b*) A. Palacios, S. Titos-padilla, J. Ruiz, J. M. Herrera, S. J. A. Pope, E. K. Brechin and E. Colacio, *Inorg. Chem.*, 2014, **53**, 1465–1474; (*c*) A. Upadhyay, C. Das, S. Vaidya, S. K. Singh, T. Gupta, R. Mondol, S. K. Langley, K. S. Murray, G. Rajaraman and M. Shanmugam, *Chem. – Eur. J.*, 2017, **23**, 4903–4916; (*d*) I. Oyarzabal, B. Artetxe, A. Rodríguez-Diéguez, J. Á. García, J. M. Seco and E. Colacio, *Dalton Trans.*, 2016, **45**, 9712–9726; (*e*) N. C. Anastasiadis, C. D. Polyzou, G. E. Kostakis, V. Bekiari, Y. Lan, S. P. Perlepes, K. F. Konidaris and A. K. Powell, *Dalton Trans.*, 2015, **44**, 19791–19795; (*f*) M. Fondo, J. Corredoira-Vázquez, A. M. García-Deibe, J. M. Herrera and E. Colacio, *Inorg. Chem.*, 2017, **56**, 5646–5656; (*g*) I. Oyarzabal, J. Ruiz, J. M. Seco, M. Evangelisti, A. Camón, E. Ruiz, D. Aravena and E. Colacio, *Chem. – Eur. J.*, 2014, **20**, 14262–14269; (*h*) K. Griffiths, J. Mayans, M. A. Shipman, G. J. Tizzard, S. J. Coles, B. A. Blight, A. Escuer and G. E. Kostakis, *Cryst. Growth Des.*, 2017, **17**, 1524–1538; (*i*) M. Maeda, S. Hino, K. Yamashita, Y. Kataoka, M. Nakano, T. Yamamura and T. Kajiwara, *Dalton Trans.*, 2012, **41**, 13640; (*j*) P. L. Then, C. Takehara, Y. Kataoka, M. Nakano, T. Yamamura and T. Kajiwara, *Dalton Trans.*, 2015, **44**, 18038–18048; (*k*) H.-R. Wen, P.-P. Dong, S.-J. Liu, J.-S. Liao, F.-Y. Liang and C.-M. Liu, *Dalton Trans.*, 2017, 1153–1162; (*l*) J. Li, R.-M. Wei, T.-C. Pu, F. Cao, L. Yang, Y. Han, Y.-Q. Zhang, J.-L. Zuo and Y. Song, *Inorg. Chem. Front.*, 2017, **4**, 114–122; (*m*) S. T. Abtab, M. C. Majee, M. Maity and R. Boc, *Inorg. Chem.*, 2014, **53**, 1295–1306; (*n*) H. L. C. Feltham, Y. Lan, F. Klöwer, L. Ungur, L. F. Chibotaru, A. K. Powell and S. Brooker, *Chem. – Eur. J.*, 2011, **17**, 4362–4365; (*o*) A. Z. Lekuona, J. Cepeda, I. Oyarzabal, A. R. Diéguez, J. A. García, J. M. Seco and E. Colacio, *CrystEngComm*, 2017, **19**, 256–264; (*p*) C. E. Burrow, T. J. Burchell, P. H. Lin, F. Habib, W. Wernsdorfer, R. Clérac and M. Murugesu, *Inorg. Chem.*, 2009, **48**, 8051–8053; (*q*) S. Das, K. S. Bejoymohandas, A. Dey, S. Biswas, M. L. P. Reddy, R. Morales, E. Ruiz, S. T. Padilla, E. Colacio and V. Chandrasekhar, *Chem. – Eur. J.*, 2015, **21**, 6449–6464; (*r*) J. Goura, E. Colacio, J. M. Herrera, E. A. Suturina, I. Kuprov, Y. Lan, W. Wernsdorfer and Vadapalli Chandrasekhar, *Chem. – Eur. J.*, 2017, **23**, 16621–16636.

24 E. M. Pineda, N. F. Chilton, F. Tuna, R. E. P. Winpenny and E. J. L. McInnes, *Inorg. Chem.*, 2015, **54**, 5930–5941.

25 (*a*) A. Barge, M. Botta, U. Casellato, S. Tamburini and P. A. Vigato, *Eur. J. Inorg. Chem.*, 2005, 1492–1499; (*b*) H. Wang, W. Cao, T. Liu, C. Duan and J. Jiang, *Chem. – Eur. J.*, 2013, **19**, 2266–2270.

26 (*a*) J. Goura, J. Brambleby, P. Goddard and V. Chandrasekhar, *Chem. – Eur. J.*, 2015, **21**, 4926–4930; (*b*) C. Liu, D. Zhang, X. Hao and D. Zhu, *Chem. – Asian J.*, 2014, **9**, 1847–1853; (*c*) L. Zhao, J. Wu, S. Xue and J. Tang, *Chem. – Asian J.*, 2012, **7**, 2419–2423; (*d*) S. K. Langley, N. F. Chilton, L. Ungur, B. Moubaraki, L. F. Chibotaru and K. S. Murray, *Inorg. Chem.*, 2012, **51**, 11873–11881; (*e*) S. K. Langley, L. Ungur, N. F. Chilton, B. Moubaraki, L. F. Chibotaru and K. S. Murray, *Inorg. Chem.*, 2014, **53**, 4303–4315; (*f*) A. V. Funes, L. Carrella, E. Rentschler and P. Albores, *Dalton Trans.*, 2014, **43**, 2361–2364; (*g*) J. Goura, J. Brambleby, C. V. Topping, P. A. Goddard, R. S. Narayanan, A. K. Bar and V. Chandrasekhar, *Dalton Trans.*, 2016, **45**, 9235–9249; (*h*) A. V. Funes, L. Carrella,

E. Rentschler and P. Alborés, *Dalton Trans.*, 2014, **43**, 2361–2364; (*i*) S. K. Langley, N. F. Chilton, B. Moubaraki and K. S. Murray, *Inorg. Chem.*, 2013, **52**, 7183–7192; (*j*) S. K. Langley, N. F. Chilton, B. Moubaraki and K. S. Murray, *Chem. Commun.*, 2013, **49**, 6965–6967.

27 (*a*) H. M. Dong, Y. Li, Z. Y. Liu, E. C. Yang and X. J. Zhao, *Dalton Trans.*, 2016, **45**, 11876–11882; (*b*) C. K. Terajima, H. Miyasaka, A. Saitoh, N. Shirakawa, M. Yamashita and R. Clérac, *Inorg. Chem.*, 2007, **46**, 5861–5872; (*c*) V. Chandrasekhar, P. Bag, W. Kroener, K. Gieb and P. Müller, *Inorg. Chem.*, 2013, **52**, 13078–13086.

28 A. Upadhyay, C. Das, S. Vaidya, S. K. Singh, T. Gupta, R. Mondol, S. K. Langley, K. S. Murray, G. Rajaraman and M. Shanmugam, *Chem. – Eur. J.*, 2017, **23**, 4903–4916.

29 (*a*) N. F. Chilton, D. Collison, E. J. McInnes, R. E. P. Winpenny and A. Soncini, *Nat. Commun.*, 2013, **4**, 2551; (*b*) J. D. Rinehart and J. R. Long, *Chem. Sci.*, 2011, **2**, 2078–2085; (*c*) C. Das, A. Upadhyay, S. Vaidya, S. K. Singh, G. Rajaraman and M. Shanmugam, *Chem. Commun.*, 2015, **51**, 6137–6140; (*d*) J.-L. Liu, Y.-C. Chen, Y.-Z. Zheng, W.-Q. Lin, L. Ungur, W. Wernsdorfer, L. F. Chibotaru and M.-L. Tong, *Chem. Sci.*, 2013, **4**, 3310–3316.

30 (*a*) V. Chandrasekhar, A. Chakraborty and E. C. Sañudo, *Dalton Trans.*, 2013, **42**, 13436–13443; (*b*) A. Chakraborty, J. Goura, P. Bag, A. K. Bar, J. P. Sutter and V. Chandrasekhar, *Dalton Trans.*, 2016, **45**, 17633–17643.

31 (*a*) J. P. Costes, S. TitosPadilla, I. Oyarzabal, T. Gupta, C. Duhayon, G. Rajaraman and E. Colacio, *Chem. – Eur. J.*, 2015, **21**, 15785–15796; (*b*) T. Gupta and G. Rajaraman, *J. Chem. Sci.*, 2014, **26**, 1569–1579.

32 J. P. Costes, S. T. Padilla, I. Oyarzabal, T. Gupta, C. Duhayon, G. Rajaraman and E. Colacio, *Inorg. Chem.*, 2016, **55**, 4428–4440.

33 I. Oyarzabal, J. Ruiz, E. Ruiz, D. Aravena and J. M. Seco, *Chem Commun.*, 2015, **51**, 12353–12356.

34 (*a*) S. K. Langley, C. Le, L. Ungur, B. Moubaraki, B. F. Abrahams, L. F. Chibotaru and K. S. Murray, *Inorg. Chem.*, 2015, **54**, 3631–3642; (*b*) S. K. Langley, D. P. Wielechowski, V. Vieru, N. F. Chilton, B. Moubaraki, L. F. Chibotaru and K. S. Murray, *Chem. Sci.*, 2014, **5**, 3246–3256.

35 (*a*) T. Gupta, M. F. Beg and G. Rajaraman, *Inorg. Chem.*, 2016, **55**, 11201–11215; (*b*) J. Long, E. Mamontova, V. Freitas, D. Luneau, V. Vieru, L. F. Chibotaru, R. A. Ferreira, G. Félix, Y. Guari, L. D. Carlos and J. Larionova, *RSC Adv.*, 2016, **6**, 10881–10888.

36 (*a*) S. K. Singh, T. Gupta, L. Ungur and G. Rajaraman, *Chem. – Eur. J.*, 2015, **21**, 13812–13819; (*b*) S. K. Singh, T. Gupta, L. Ungur and G. Rajaraman, *Inorg. Chem.*, 2014, **53**, 10835–10845.

37 (*a*) E. Ruiz, S. Alvarez, A. Rodriguez-Fortea, P. Alemany, Y. Pouillon and C. Massobiro, *Magnetism: Molecules to Materials II*, ed. J. S. Miller and M. Drillon, 2001; (*b*) A. Bencini, F. Totti, C. A. Daul, K. Doclo, P. Fantucci and V. Barone, *Inorg. Chem.*, 1997, **36**, 5022–5030.

38 (*a*) K. R. Vignesh, S. K. Langley, K. S. Murray and G. Rajaraman, *Inorg. Chem.*, 2017, **56**, 2518–2532; (*b*) K. R. Vignesh, S. K. Langley, K. S. Murray and G. Rajaraman, *Chem. – Eur. J.*, 2017, **23**, 1654–1666.

39 (*a*) Y. Y. Zhu, Y. Q. Zhang, T. T. Yin, C. Gao, B. W. Wang and S. Gao, *Inorg. Chem.*, 2015, **54**, 5475–5486; (*b*) A. V. Funes, L. Carrella, L. Sorace, E. Rentschler and P. Alborés, *Dalton Trans.*, 2015, **44**, 2390–2400; (*c*) V. Chandrasekhar, A. Dey, A. J. Mota and E. Colacio, *Inorg. Chem.*, 2013, **52**, 4554–4561; (*d*) A. Ferguson, A. Parkin, J. Sanchez-Benitez, K. Kamenev, W. Wernsdorfer and M. Murrie, *Chem. Commun.*, 2007, 3473–3475; (*e*) S. Manna, A. Bhunia, S. Mistri, J. Vallejo, E. Zangrando, H. Puschmann, J. Cano and S. C. Manna, *Eur. J. Inorg. Chem.*, 2017, 2585–2594.

